Solar RRL
www.solar-rrl.com

The Non-Innocent Role of Hole-Transporting Materials in Perovskite Solar Cells

Francesco Lamberti, Fabian Schmitz, Wei Chen, Zhubing He,* and Teresa Gatti**

The race to the future generation of low-cost photovoltaic devices continuously takes on added momentum with the appearance of novel practical solutions for the fabrication of perovskite solar cells (PSCs), a paradigm technology for ultracheap light-to-electricity conversion. Much has been done in the past few years toward defining standard protocols for the assessment of their efficiency and stability, aiming at achieving a worldwide consensus on the issue, that will allow reliable reporting of new data. While this is undoubtedly a step ahead toward commercialization of these devices, it also often triggers researchers to test record architectures using benchmark configurations, mainly for what regards the ancillary layers that extract electrical charges from the photoexcited perovskite. In particular, the mostly used hole-transporting material (HTM) is the small-molecule spiro-OMeTAD, which is also well known to be the origin of PSC degradation after prolonged operation. Herein, it is aimed to remark the huge impact of the HTM on PSC performance, recalling major issues associated with the conventional spiro-based one and providing an overview of state-of-the-art alternatives. Finally, possible scenarios for the future development of smart HTMs are also envisioned, as charge-extracting layers, with a real active role in ensuring PSC operational stability.

1. Introduction

Spiro-OMeTAD (2,2′,7,7′-tetrakis[*N*,*N*-di(4-methoxyphenyl)amino]-9,9′-spirobifluorene, from now on simply Spiro) is the most used and applied hole-transporting material (HTM) in perovskite solar cells (PSCs). The reason is straightforward: after opportune formulation (i.e., addition of 4-*tert*-butylpyridine, tBP, and lithium bis(trifluoromethylsulfonyl)-imide, LiTFSI, as dopants/additives), the planar PSCs normally achieve the highest power conversion efficiencies (PCEs) at lab scale (up to 24%).[1] However, this result is strongly overestimated when compared with the long-term stability of the device: it has been already largely proved by several works that the necessary doping of the organic material augments the hygroscopic character of the layer, thus favoring moisture uptake from the atmosphere and subsequent perovskite film decomposition.[2,3] Combined with its notable cost (nowadays slightly decreasing due to the presence of more producers on the market),[4,5] we can assert that Spiro is only a model/benchmark HTM useful for lab-scale PSC production and testing. This is a pity indeed, because it possesses all the properties required for a good performing HTM: the high glass transition temperature due to the Spiro-type bond, the smooth film morphology that it forms, the relative simple processing, the electrochemical stability, the optical transparency in the visible window, the amorphous nature, the optimal band alignment with the perovskite valence band, and the chemical compatibility with dopants. Despite these very promising properties therefore, the high costs and very low inherent hole conductivity hugely reduce the possible commercialization of Spiro-based PSCs and force scientists to identify new avenues for obtaining long-term stability and for simplifying device processing methods.

F. Lamberti
Department of Chemical Sciences
University of Padova
via Marzolo 1, 35131 Padova, Italy
E-mail: francesco.lamberti@unipd.it

F. Lamberti
Interdepartmental Centre Giorgio Levi Cases for Energy Economics and Technology
University of Padova
via Marzolo 9, 35131 Padova, Italy

The ORCID identification number(s) for the author(s) of this article can be found under https://doi.org/10.1002/solr.202100514.

DOI: 10.1002/solr.202100514

F. Schmitz, T. Gatti
Center for Materials Research
Justus Liebig University Giessen
Heinrich Buff Ring 17, 35392 Giessen, Germany
E-mail: teresa.gatti@phys.chemie.uni-giessen.de

W. Chen, Z. He
Department of Materials Science and Engineering, Shenzhen Key Laboratory of Full Spectral Solar Electricity Generation (FSSEG)
Southern University of Science and Technology
Xueyuan Rd. 1088, 518055 Shenzhen, China
E-mail: hezb@sustech.edu.cn

After proper molecular structure engineering through the introduction of methoxy groups, allowing to reach the ideal melting temperature (≈121 °C),[6] the subsequent engineering of the Spiro-HTM formulation underwent two different routes: reducing the effect of the environment by replacing the additives (e.g., with cobalt-based complexes[7]) and optimizing the energy matching with the perovskite films.[8] Beyond these experimental strategies, other organic compounds were adopted as HTMs, such as poly(3,4-ethenedioxythiophene):poly(styrenesulfonate) (PEDOT:PSS), the most implemented HTM in inverted and flexible PSC architectures due to its very low processing temperature,[9] polytriarylamine (PTAA), going from 16.2%[10] up to 20.2%[11] PCE in few years, or (poly[(9,9-dioctyl-fluorenyl-2,7-diyl)-co- (4,4′-(*N*-(4-secbutylphenyl) diphenylamine)]) (TFB)[12] with the overall goal to diminish electrical hysteresis and improve the conductivity of the HTM without the use of any dopants. In addition, HTM–perovskite interface tuning through 2D/3D engineering also allowed to open up new perspectives for remarkable device stability improvement and elimination of dopants from the hole-extracting layer.[13]

At the same time, inorganic semiconductors, mainly oxides, were applied to both inverted and direct architectures: materials like NiO_x,[14] CuI,[15] CuO_x,[16] V_2O_x,[17] MoO_x,[18] MoS_2,[19] CuSCN[20] became competitors of Spiro-based HTMs. The use of inorganic semiconductors prevents the chemical degradation occurring in organic HTMs after light soaking and prolonged use. In particular, detrimental effects of nitrogen, oxygen, and moisture were proven to be effective when organic HTMs were used.[21,22] In a recent paper, some of us also showed that instability can be due to a direct action of the additives in a classical Spiroformulation: oxygen soaking coupled to the contemporary presence of tBP and LiTFSI, fundamental for achieving the highest conductivity in Spirolayers, ultimately causes a dedoping process with the formation of a pyridinium cation (see the next paragraph for more details).[23] However, inorganic HTMs do not guarantee to date the same conductivities and ease of processing of organic molecules: are we thus at a dead end? How can we exploit the benefits of organic HTMs without neglecting the long-term stability that is vital for commercialization within the design of next-generation HTMs? In this Review, we want to highlight the most recent efforts reported in the literature that display unique properties for HTMs able to provide both a functional and an active role in the device fortune, that is, emphasizing the "noninnocent" role of HTMs in PSCs. Leveraging on Spiro-based HTMs intrinsic limitations, we will review the most innovative alternatives, starting from dopant-free and fully inorganic HTMs, to then discuss even more promising possibilities, such as those deriving from HTMs-free carbon-based PSCs (C-PSCs) and "smart" HTMs that display intriguing properties able to actively cope with specific stability issues (**Figure 1**).

2. Dopant-Free HTMs for PSCs

As discussed previously, the need to use LiTFSI as the dopant to trigger the oxidation of Spiro-based HTM formulations[24] has been shown to be a key issue for device stability, due the hygroscopic quality of the finally obtained layer, causing an undesirable water uptake from the atmosphere that ultimately reaches the perovskite photon absorber, causing its degradation toward the high-bandgap metal halide precursors.[25] While much attention has been addressed to the role of this ionic additive in influencing PSC stability, less was known until few years ago about the possible influence of the second major additive in the Spiro-HTM formulation, namely, the small organic molecule *t*BP. This additive is generally assumed to provide considerable help in reaching the optimal HTM morphology on top of the perovskite layer, permitting good pinhole passivation. In contrast, it is used in large excess with respect to Spiro-molecules in the HTM blend (about three times more) and it has a very high boiling point (197 °C), excluding the possibility that it leaves the layer after casting through evaporation. In 2019, some of us fully demonstrated, following previous reports that hinted at the same conclusion but did not fully explain the mechanism behind,[3,26] that such additives have indeed the ability to cause progressive dedoping of Spiro-HTMs, thus altering the charge transport properties.[27] To investigate this ageing process, we used electron spin resonance (ESR) spectroscopy, a technique very sensitive to the presence of unpaired radicals in samples and of their surrounding environment. Being the doped Spiro-molecule, a radical cation, we could very nicely follow the decay of its ESR signal

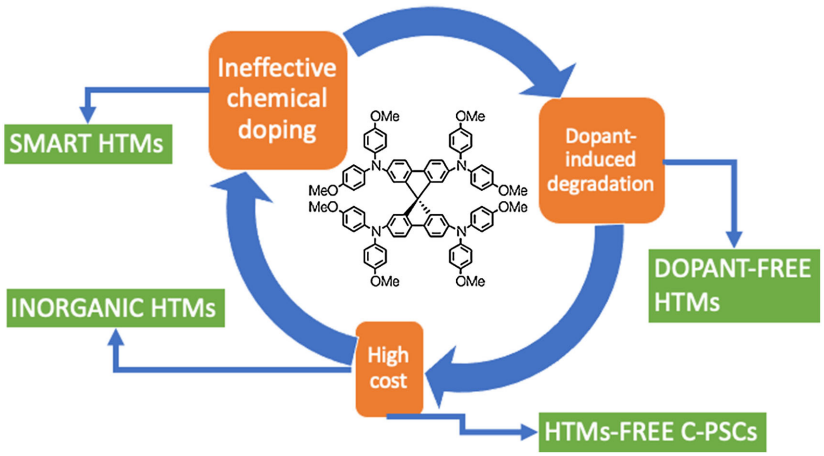

Figure 1. Main drawbacks associated with Spiro-OMeTAD HTMs for PSCs and possible solutions to circumvent them examined in this Review.

in different conditions (**Figure 2**a). With the help of Raman spectroscopy then, we were able to unequivocally identify the existence of pyridinium ions as the residual products existing in the Spiro:LiTFSI:*t*BP mixture after the ESR signal of the Spiro radical cation completely disappeared (Figure 2b). Based on these evidences, we proposed a dedoping mechanism for Spiro$^+$ molecules that pass through the formation of an unstable *t*BP radical cation, which then further reacts with another Spiro$^+$ species to produce a *t*-butylpyridinium adduct (Figure 2c).

It is evident from all the earlier discussed aspects that doping of small-molecule-based HTMs cannot most likely represent an adoptable solution in future commercialized PSCs. In this sense, many efforts from chemists and materials scientists have been addressed in the past few years at developing other small molecules that can extract and transport holes efficiently without requiring a doping step (dopant-free HTMs). Molecular engineering has provided a plethora of new structures exploiting different strategies to improve hole mobility such as donor–acceptor (D–A) alternation or extended π-conjugation. This specific topic has been anyway thoroughly addressed in other seminal reviews—we address the reader interested in understanding more of this particular aspect.[28,29] Here, we will just report some peculiar and very recent examples that might constitute the bases for next improvements in the field.

Some of us reported recently on new small-molecule structures characterized by an advanced and very accurate design, able to address multiple requirements and functions for an ideal dopant-free molecular HTM to be used in inverted PSC architectures.[30] In **Figure 3**a, such a design strategy is highlighted, showing that together with the unmissable hole transport properties, dipole moment tuning (which can induce self-doping and built-in potential to boost charge extraction—more on this topic is discussed in Section 5), appropriate π-stacking (to improve charge mobility), and ability to passivate perovskite surface defects are additional powerful features installed in the newly developed molecules (namely, MPA-BTI and MPA-BTTI). With similar compounds, p–i–n devices reached a remarkable maximum PCE of 21.17%, with negligible hysteresis and superior stability under prolonged illumination. A further step is the development of similar structures, brought to the synthesis of dendritic derivatives like the ones shown in Figure 3b.[31] Here, the central acceptor moiety is decorated with either diphenylamine, carbazole, or diphenylamine-/carbazole-mixed dendrons that act as the donor components. With these dendrimers, structures which are located in the middle between small molecules and polymers, excellent HTM film morphology was achieved, allowing good interfacial contacts with the overlaying perovskite layer and providing PCEs above 20%, with exceptionally ultrahigh fill factor (FF) values.

The most recent trends in small-molecule-based dopant-free HTMs have shown evergrowing attention in the direction of always more complex chemical engineering, with remarkable reports on species able to conduct multisite defect healing at the perovskite/HTM interface, allowing application in solar modules,[32] to adopt face-on orientation on the perovskite surfaces to provide high hole mobilities[33,34] or tune aggregation states and intermolecular interactions depending on peripheral substituents that influence PCE and device stability,[35,36] also in inverted PSCs.[37]

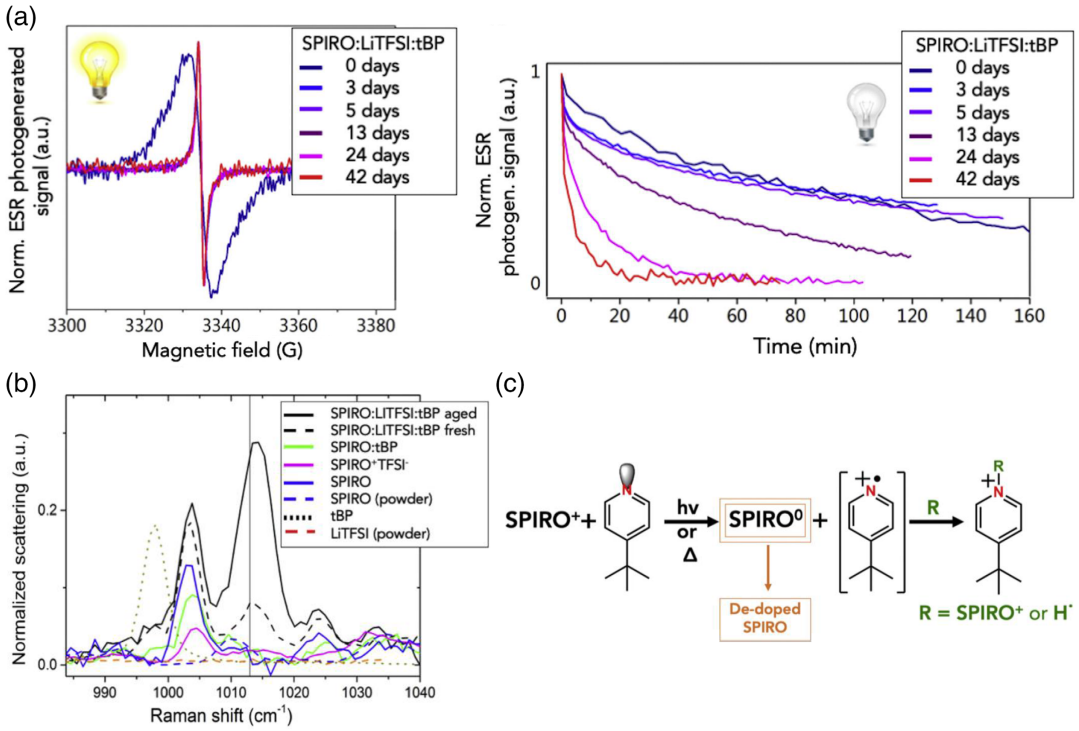

Figure 2. Spiro-OMeTAD dedoping process triggered by the *t*BP additive. a) ESR investigation of the dedoping process. b) Raman spectra of the aged samples showing the presence of an intense pyridinium ion signal. c) Proposed mechanism for dedoping. Reproduced with permission.[27] Copyright 2019, Elsevier Inc.

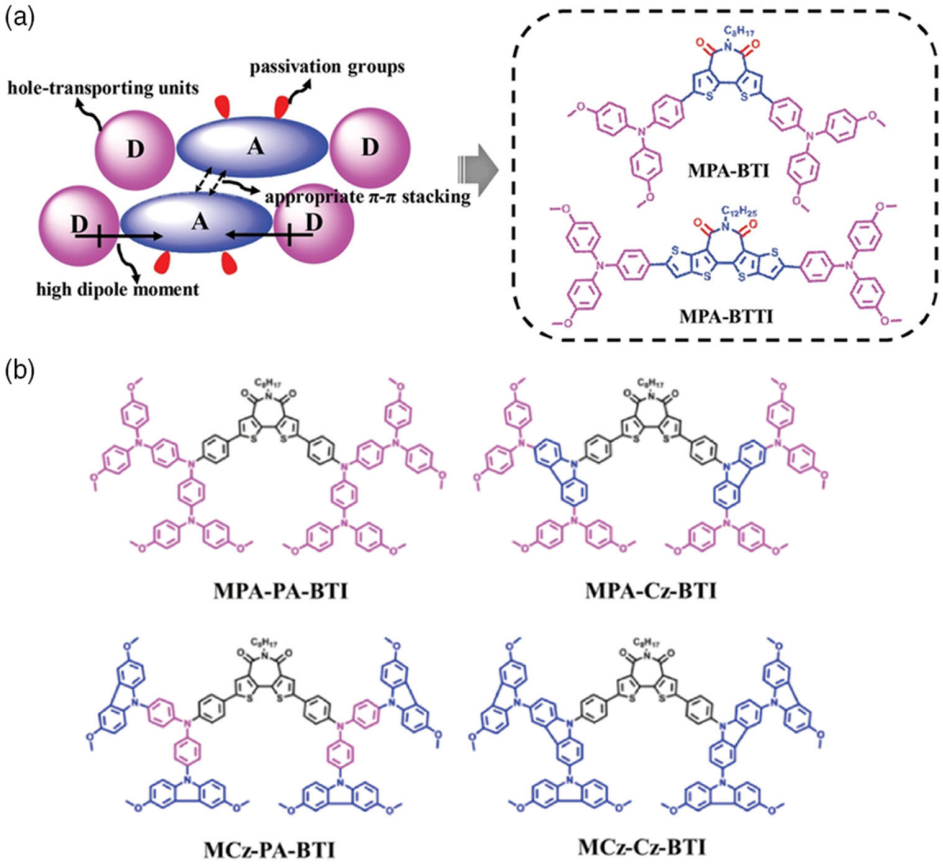

Figure 3. Emerging dopant-free small-molecule HTMs for inverted PSCs. a) Molecular design principle for D-A-D dopant-free molecular HTMs with reinforced π-stacking, high dipole moment, and perovskite passivation ability. Reproduced with permission.[30] Copyright 2019, Wiley-VCH. b) Structures of D-A-D dopant-free dendritic HTMs. Adapted with permission.[31] Copyright 2020, Science China Press and Springer-Verlag GmbH.

An alternative strategy to overcome the dopant-related bottleneck is to resort to composite materials as HTMs. This approach can rely on the choice of a suitable matrix, which is perhaps already a good organic HTM, in which fillers like nanomaterials or small molecules are inserted, that have a positive influence on the overall conductivity of the matrix and thus somehow act as dopants, even if they do not hold the previously discussed drawbacks of classical ones, like lithium salts. For example, nanocarbon species like carbon nanotubes (CNTs) or graphene-based materials (GBMs) can be selected for the role of conducting fillers, when their optimal dispersion within HTM matrix is attainable. In this way, HTMs which normally perform worse than Spiro in terms of overall PCE they allow to deliver, like poly(3-hexylthiophene) (P3HT), can be endowed with augmented transport properties. P3HT composites containing CNTs as HTMs in direct-architecture PSCs were first proposed by Wang and coworkers[38] and characterized by significantly reduced charge recombination at the interface with the perovskite layer compared with bare P3HT, which consequently provided higher PCEs due to improved open-circuit voltage (V_{OC}) and FF. In 2016 then, some of us reported on the use of highly homogeneous P3HT composite HTMs with organic functionalized CNTs and GBMs, where the optimized concentration of carbon nanostructures to ensure the best dispersibility in the polymer matrix was determined by applying a sedimentation-based separation (SBS) process before HTM deposition, thus eliminating all major aggregates that can act as sources of charge recombination within the thin layer.[39] With these HTMs, both efficiency and long-term stabilities of the resulting PSCs were improved compared with the use of pristine P3HT. As the organic functionalization in this blend approach seemed to have a significant role in defining the final quantity of well-dispersed nanocarbons within the polymer phase after application of the SBS process, we further investigated the effect of different functionalization moieties able to establish supramolecular interactions with the P3HT matrix and, more specifically, with either the lateral alkyl chains or the thiophene-based polymeric backbone (**Figure 4**a).[40] From this systematic screening of functionalized GBM derivatives, two composites resulted in having the higher stabilized concentrations of fillers in the polymer blend after SBS and those were namely the derivatives bearing aryl-bithiophene and aryl-hexyloxy moieties, which were consequently tested for the role of HTMs in n–i–p solar devices in comparison with pure P3HT and Spiro-based HTMs. As the performance of the two types of composites in PSCs resulted in being significantly different, with the derivative containing the bithiophene functionalities providing lower PCEs (even lower than bare P3HT) as a consequence of reduced short-circuit

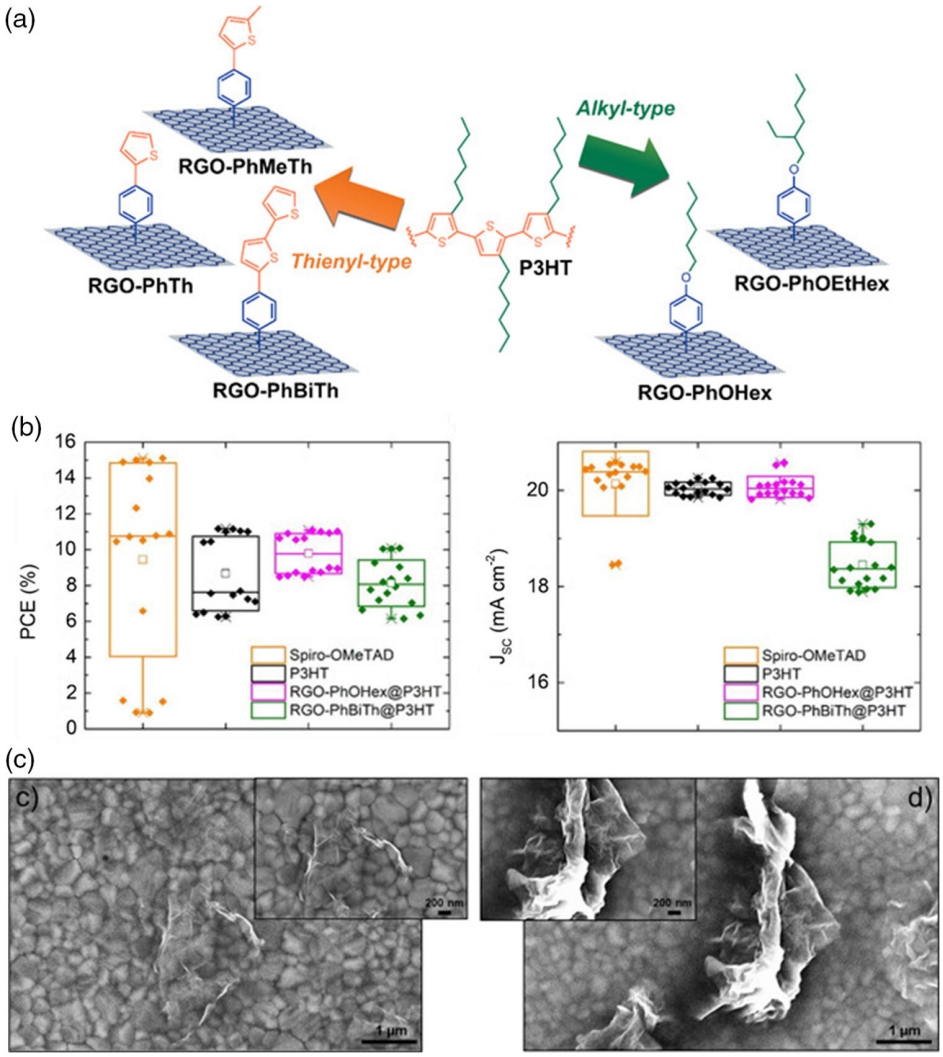

Figure 4. Use of organic-functionalized reduced graphene oxide (RGO) fillers in a P3HT matrix for the construction of composite HTMs. a) Different functionalities address supramolecular interactions with the semiconducting polymer matrix and allow to obtain high concentrations of the carbon nanostructure in a polymer blend without the concomitant formation of aggregates. b) PSC performance is strongly affected by the type of functionality covalently attached to RGO. c) Lower PCEs and J_{SC} in bithiophene-functionalized RGO/P3HT HTMs are due to self-aggregation of the RGO flakes (right SEM image) that generate short circuits within the charge-extracting layer, ultimately affecting charge recombination. In contrast, the presence of hexyl moieties on the nanocarbon favors flat disposition of the sheets in the polymer matrix, allowing improved hole extraction and transport across the HTM. Adapted with permission.[40] Copyright 2018, Wiley-VCH.

current densities (J_{SC}, Figure 4b), we investigated the morphology and electrical properties of the perovskite/HTM interface by means of scanning electron microscopy (SEM) and impedance spectroscopy. In this way, we were able to evidence increased charge recombination occurring in this down-performing HTM case, due to the self-crumpling of the GBM flakes within the polymer matrix (Figure 4c), generating local short circuits that funnel back to the perovskite and the extracted holes. In contrast, the presence of hexyl chains on the GBM filler seems to favor the smooth displacement of the nanocarbon sheets within the P3HT HTM, favoring charge extraction and transport.

The versatility of P3HT to host nanofillers of various natures, together with its relatively low price, high hydrophobicity, and ease of processability/film-forming ability, has stimulated several other attempts to design and prepare innovative polymer composite HTMs to improve PSC performance and stability. Xu and coworkers reported on three different types of P3HT composite HTMs tested in n–i–p device configuration.[41–43] In the first work, they prepared P3HT/phtalocyanine nanowire composites tuning the ratio between the two components to achieve a modulation of both HTM energy levels and hole mobility (**Figure 5**a).[41] With these composite HTMs, better efficiency was obtained in as-prepared PSCs compared with the use of pristine P3HT as HTM and, more strikingly, also remarkable long-term stability resulted for devices kept unencapsulated in high-humidity conditions (Figure 5a). In another work, the same group reported a similar blending approach between P3HT and a highly hydrophobic Lewis acid small molecule, namely,

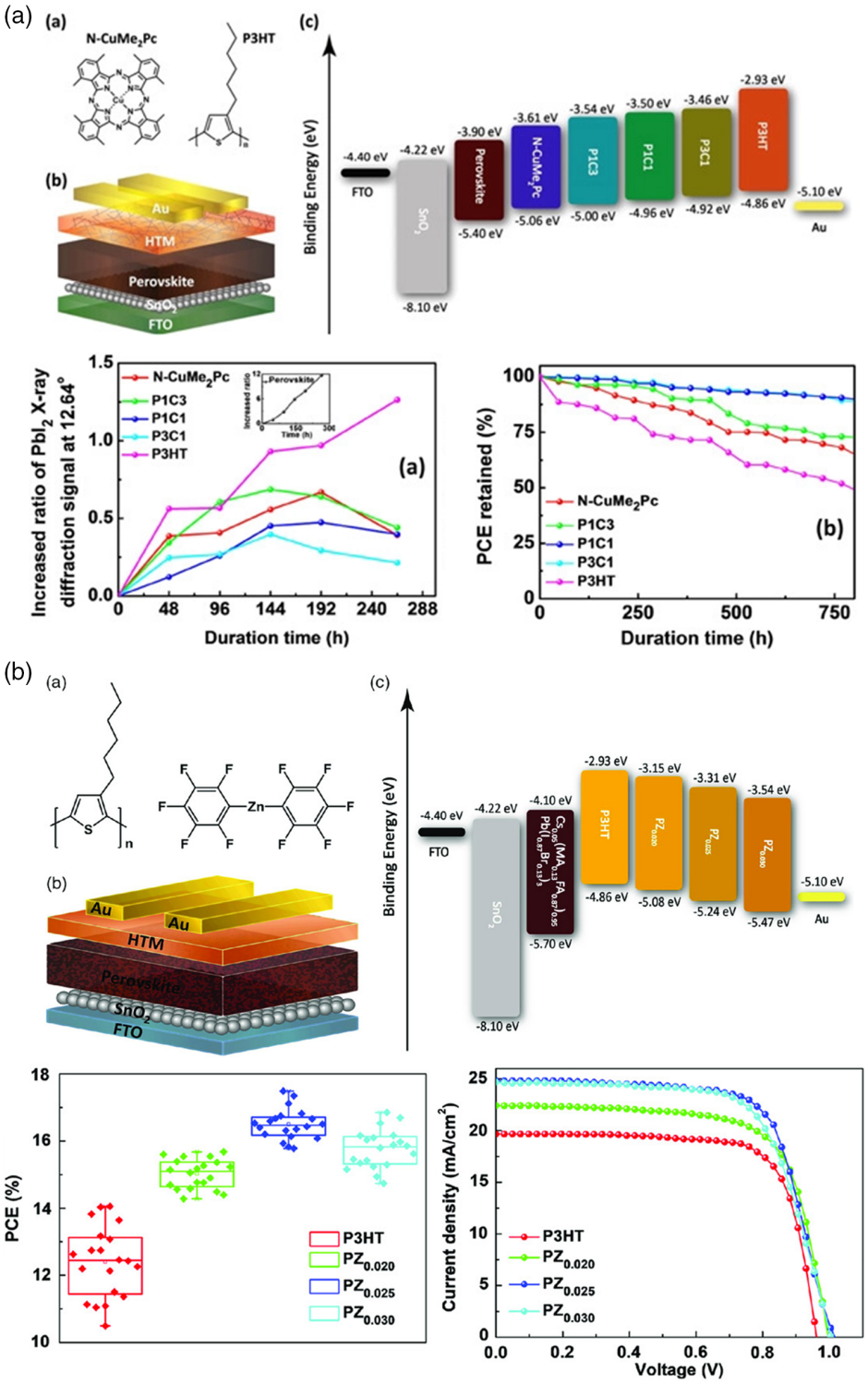

Figure 5. Examples of P3HT composite HTMs with different small molecules acting as highly hydrophobic dopants. a) P3HT composite HTMs with copper(II) phtalocyanine (*N*-CuMe$_2$Pc) nanowires at different polymer:nanowire ratios (P1C3, P1C1, P3C1) are used in direct-architecture PSCs, providing interesting environmental stability profiles compared with the use of the sole pristine polymer. Reproduced with permission.[41] Copyright 2018, Wiley-VCH. b) P3HT composite HTMs with a bis(pentafluorophenyl)zinc Lewis acid at different dopant concentrations providing improved performance in n–i–p devices compared with pristine P3HT. Reproduced with permission.[42] Copyright 2019, Wiley-VCH.

bis(pentafluorophenyl)zinc, to achieve doping of the polymer and consequently higher PCEs in PSCs as a consequence of improved hole mobility and hole extraction ability (Figure 5b).[42]

Finally, it should be mentioned that the mixing of p-type semiconducting polymers with phtalolocyanines into composite HTM structures has provided also other interesting results in terms of PSC performance enhancement. P3HT composites with either Zn or Cu phtalocyanines were used recently to, respectively, improve efficiency in carbon-based PSCs[44] (see discussion on these particular devices in Section 4) and deliver outstanding FF values and thermal stabilities in large-area nanostructured PSCs.[45] In a p–i–n configuration, poly(3,4-ethylenedioxythiophene):polystyrenesulfonate (PEDOT:PSS) composites with Cu phtalocyanines as HTMs delivered a maximum PCE above 17% with high FF, due to excellent hole extraction capability and improved perovskite crystallization on top of the composite layer.[46]

3. Inorganic HTMs for PSCs

A huge number of works discussing the integration of inorganic HTMs in PSCs are present in literature.[47–49] The reason for this wide interest in similar layers/materials is certainly related to the numerous inorganic compounds that can be applied for this role, their relative ease of processing through versatile technologies (spin coating, spray coating, thermal evaporation, electrospraying), the low cost associated with high-abundant raw materials, and the inherent hydrophobic nature of many of them, which prospects good device stability. In addition, further benefits can be derived by the interfacing of inorganic HTM layers with organic ones, enabling higher levels of control of the hole-extracting properties.[50] Particular mention should be given to bidimensional transition metal dichalcogenides (2D TMDs), whose use in HTMs has been thoroughly discussed in a recent review.[51] For this reason, in this brief overview, we will highlight only the last remarkable results concerning the use of inorganic HTMs, trying to give emphasis to the functional role of the HTM layer itself with respect to the overall device performance.

The mostly used materials are the ones belonging to the copper family: CuO_x, CuSCN, CuI. Historically, they were first extensively applied to dye-sensitized solar cells (DSSCs)[52] and then (as occurred many times in PSC history, directly derived from DSSC research) applied also to PSCs. Researchers active in the field are indeed very lucky: copper is a wonderful element because it is abundant on Earth and does not show any major safety issue for humans and the environment (for this reason it is considered as a noncritical raw material),[53] so, most likely, next-generation solar devices will be realized, exploiting copper-based compounds and other noncritical transition metals like iron or manganese.[54] Copper materials are economical and chemically stable, with proper energy levels for alignment with perovskite photoactive layers and optimal transmittance. In particular, copper oxides, CuO_x, different from the other species of the family, have a very narrow bandgap and thanks to its p-conductivity it has been extensively used for the so-called all-oxide solar cells,[54,55] in which it acts as the absorbing layer. However, hole conductivity is not so high, forcing researchers to adopt doping strategies when preparing such solar devices. In the perovskite field, however, these materials are generally used in the pristine form. The first example of Cu_2O as HTM in a PSC provided about 9% PCE[56]: cuprous oxide was deposited by magnetron sputtering, a methodology that allows fine tuning of the oxygen percentage in the prepared thin film but, conversely, does not allow to obtain the highest crystallinities required for high FFs. For these limitations, copper oxide-based PSCs have generally very low efficiencies (below 10%).[48] More suitable for perovskite photovoltaics (PV) is copper iodide, CuI, because it has good solubility in organic solvents (thus making it a perfect candidate for replacing Spiro or as a dopant replacing hygroscopic LiTFSI[57]), a good hole mobility (up to 20 $cm^2 V^{-1} s^{-1}$),[58] and a high bandgap (3.1 eV) acting as the blocking layer for interfacial charge recombination. However, also in this case, the obtainable PCE does not exceed 10% due to lower V_{OC} values than those provided using Spiro as reference, although FF is higher.[59] To the best of our knowledge, however, there is only one example in which an engineered CuI HTM allowed to reach almost 20% PCE[60]: in this work Ye et al., by exploiting molecular engineering, realized for the first time a p-type semiconductor including thiourea in the CuI structure, increasing the PCE from 14.6% to 19.9%. The authors explained this result by an ongoing perovskite trap passivation conducted by the thiourea additives.

The main character in the copper family is undoubtedly copper thiocyanate, CuSCN, that displays all the good properties of a suitable HTM for PSCs[61]: decent hole mobility due to the quasimolecular structure given by the pseudohalide SCN^-,[62] high bandgap (3.4–3.9 eV), p-type character (work function [WF] of 5.2 eV), hydrophobic nature and good solubility in organic solvents (mainly sulfides) and aqueous ammonia.[63] In this latter case, researchers demonstrate the possibility of integrating CuSCN in a water environment, paving the way to scalable manufacturing of PSCs using mild solvents and obtaining a remarkable PCE of 17.5%. In addition, CuSCN filmability is very straightforward due to its lamellae-like structure, bringing reduced surface roughness. CuSCN can well be combined with other 2D materials like graphene. Arora et al. achieved 20% PCE in a standard-architecture PSC in which the CuSCN layer was wet processed: by the addition of a thin layer of RGO between CuSCN and top-contact gold electrode, the performance of the device remained almost unchanged after 1000 h of continuous illumination at 60° (**Figure 6**a).[64] The high potential of this compound is demonstrated also by the emerging attempts of CuSCN engineering: in an early article,[65] Yang et al. optimized the interface between perovskite and CuSCN by the addition of an organic aromatic compound that facilitates hole extraction: in this way, the resulting device showed remarkable long-term stability (86% of initial PCE after 200 days). Similarly, Xu and coworkers reported a CuSCN/conjugated polymer multilayer HTM structure to achieve 21.7% certified PCE in a direct-architecture PSC and high light and moisture stability.[66]

Another promising example of copper-based HTM is copper phthalocyanine (CuPc), that recently was applied to standard-architecture PSCs using Au as top electrode[67]: in this remarkable work, the researchers found that by conducting a postannealing step at 85 °C, the recombination at the HTM/perovskite interface strongly diminishes due to Au doping of the CuPc layer that favors the dissolution of cracks in between grains, as shown in the SEM image (Figure 6b). The thermal

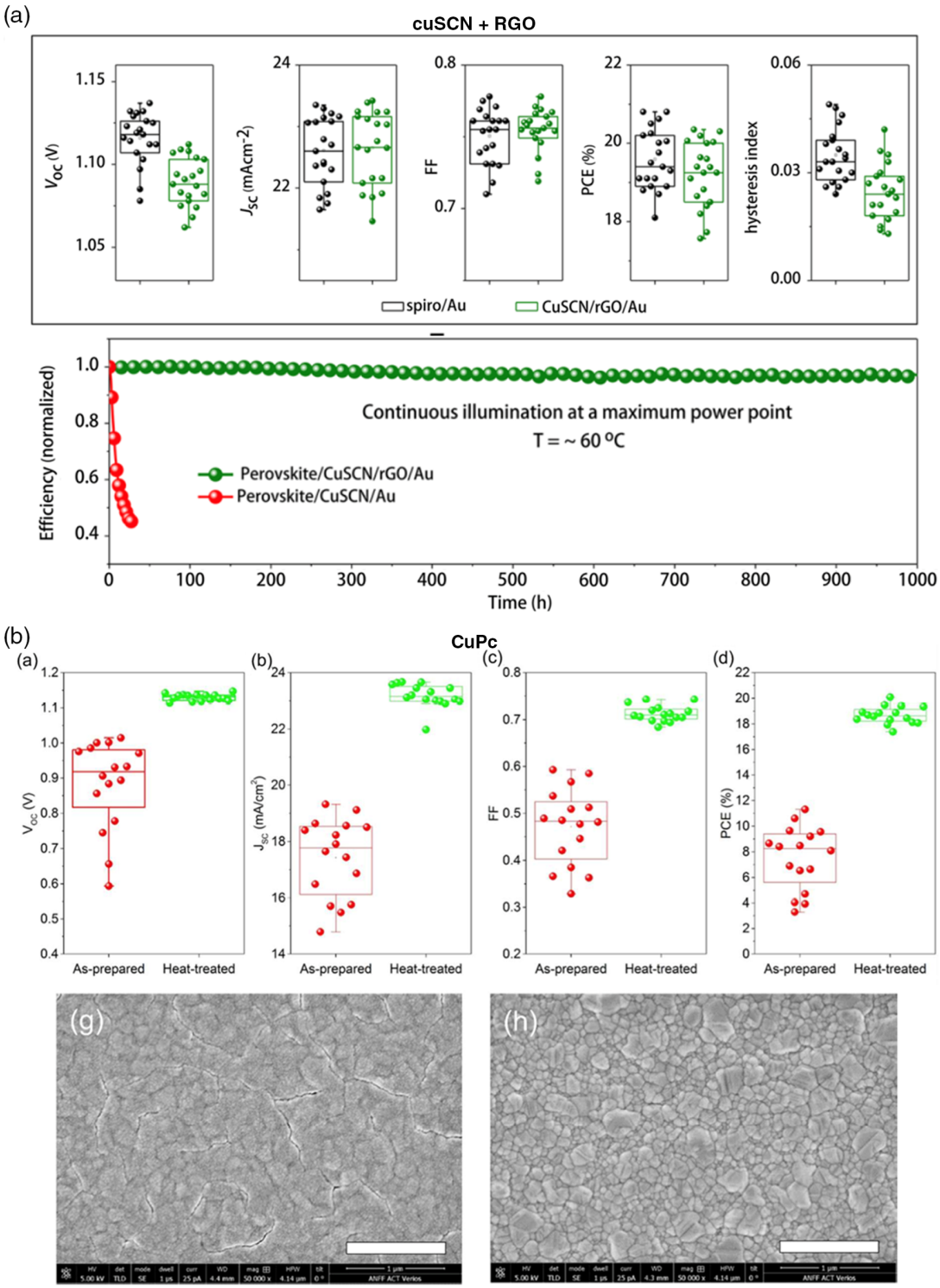

Figure 6. To-date, best-performance examples of PSCs containing copper-based HTMs. a) Long-term stability of a PSC containing a CuSCN/RGO HTM. Adapted with permission.[64] Copyright 2017, The Authors, some rights reserved; exclusive licensee American Association for the Advancement of Science. b) Effect of heat treatment on a CuPc HTM-based PSC. Adapted with permission.[67] Copyright 2018, American Chemical Society.

stability is thus hugely increased, showing almost unchanged performances after 2000 h at 85 °C.

Another example of very popular inorganic HTMs is nickel oxide, NiO. The compound is a notable candidate for replacing organic HTMs having intrinsic p-character with good hole mobility (2.8 $cm^2 V^{-1} s^{-1}$),[68] excellent transparency, optical bandgap (3.6–4 eV),[69] and valence band values in agreement with perovskite configuration, facilitating hole extraction and electron blocking.[70] It can be processed by exploiting different strategies, like sol–gel, electrodeposition, spray and spin coating, sputtering, pulsed laser deposition, and more. His fortune derives from the very-low hygroscopic and acidic nature and for this reason it is widely applied to inverted p–i–n devices. Although remarkable PCEs were reached (20%),[71–73] its use is not so extensive, and the main reason can be ascribed to the toxicity of nickel. Comprehensive detailed reviews are available in literature for further reading.[74,75]

Over the past several years, some of us have systematically investigated the optimization of NiO_x HTMs via both doping and surface passivation strategies, by which we have achieved over 22% efficiency for inverted PSCs with low-temperature-processed NiO_x-based HTMs.[76] It is well established that stoichiometric NiO is insulating, which results in increased recombination and reduced hole extraction. The conductivity of NiO_x can be increased by extrinsic dopants with shallower acceptor levels. In 2017, we demonstrated that Cs could be an effective dopant for significantly improving the conductivity and enhancement of device performances.[70] We have obtained a best efficiency over 19% based on $MAPbI_3$ perovskites. However, these Cs-doped NiO_x HTMs were prepared by a sol–gel solution method, which required high-temperature post-annealing (270 °C), limiting its application on flexible substrates and increasing the fabrication costs. To avoid high-temperature processing, we developed NiO_x nanoparticles ink recipe to prepare the NiO_x HTMs at low temperatures (<150 °C). We achieved over 18% PCE for the devices with NiO_x nanoplatelets (NPs) HTMs and $MAPbI_3$ perovskites.[77,78] To further improve performance, Cu-doped NiO_x NPs were prepared, thus increasing HTM conductivity and tailoring hole concentration and WF. The possible mechanism of Cu doping was comprehensively investigated, and the best efficiency for small-area, large-area, and flexible devices was over 20%, 18%, and 17%, respectively.[79] At a later stage, another molecular doping strategy for NiO_x with F6TCNNQ was developed, allowing to achieve over 20.8% efficiency for NiO_x-based inverted PSCs, which was the highest reported efficiency in that period.[80] More recently, we attempted the use of alkali chlorides as interfacial modifiers at the NiO_x/perovskite interfaces.[81] The role of the alkali chlorides in passivating the perovskite defects was explored experimentally and theoretically. After alkali chloride modification, the V_{OC} and PCE of the resulting inverted PSCs were significantly improved, with best PCE close to 21%.

For concluding this section on inorganic HTMs, we highlight the last works exploiting 2D TMD HTMs[51,82] exceeding the 20% PCE threshold. 2D WS_2 was applied in p–i–n devices by Liu et al.,[83] exploiting its ultrahigh hole mobility and its capability of driving high-quality epitaxial growth of the perovskite thin film, thus achieving about 21% PCE. At the same time, 2D MoS_2 flakes were adopted also in an inverted PSC in which, as in the previous example, the chalcogenides guided the anisotropic growth of the perovskite, allowing the device to reach 20.55% PCE with no hysteresis.[84] The last example that is noteworthy to highlight concerns the use of a not common HTM like MnS: like copper, manganese represents one of the noncritical metals that makes sense to try to exploit and engineer. In a recent work,[85] Chen et al. showed the possibility of retaining 90% of the initial PCE (≈20%) in a very humid environment (80% relative humidity: RH) for 1000 h, using the suboptimal perovskite methylammonium lead iodide and MnS HTM.

4. HTM-Free PSCs

A drastic, yet simple solution to overcome the drawbacks as well as the high costs of an HTM is to spare it entirely and deposit the back electrode directly on top of the perovskite layer. However, when using metallic electrodes, this method reveals new problems for the PSC performance. For example in case of the often used silver electrodes,[86–89] those limits are a large energy mismatch between the perovskite's valence band maximum (VBM) and the electrode's WF,[90] as well as the formation of silver halides at the perovskite/electrode interface, leading to a degradation of the perovskite layer itself.[91–94] Gold, another commonly used electrode material, has been observed to also negatively affect PSC performances due to ion migration of gold particles into the perovskite layer,[95] as well as the formation of gold halide complexes.[96] Furthermore, both HTMs and metal electrodes take up a large part of PSC material costs. **Figure 7** shows that eliminating the HTM and substituting a gold electrode by an abundant, easily processable material can drastically reduce the material cost of PSCs.[97]

Carbon-based materials can work as metal electrode/HTM substitutes, as they show WFs comparable with that of gold (5.1 eV),[90] are chemically inert toward the perovskite layer, and, due to the typical thickness of carbon electrodes (CEs) of several micrometers, they protect the perovskite layer from humidity, increasing the environmental stability of PSCs.[98–101] Still, there are several factors that suppress PSC efficiencies when CEs are applied that have to be targeted to boost the performance of carbon-based PSCs (C-PSCs). Those are the

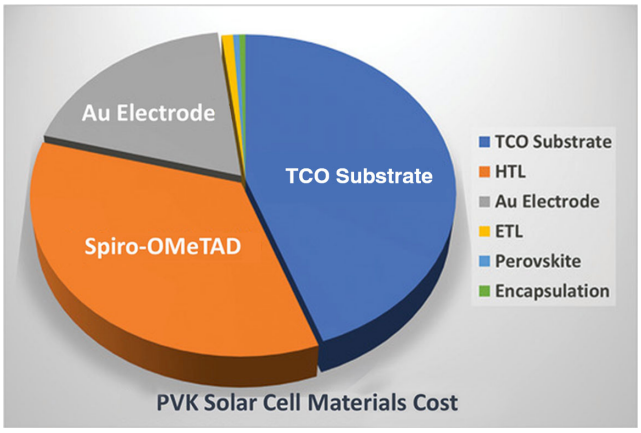

Figure 7. Relative material costs of separate PSC components. Adapted with permission.[97] Copyright 2020, Wiley-VCH.

deposition-caused inhomogeneous contact of the CE with the perovskite layer, that reduces the interfacial charge transfer,[100,102,103] as well as the anisotropic conductivity of graphene/graphite layers, characterized by low resistance along the 2D plane of individual graphene sheets but high resistance in the perpendicular direction.[102–105] CEs also lack the reflectivity of metal electrodes, which means that the thickness of a perovskite layer in a C-PSC has to be increased for it to absorb the same amount of photons as it would do when a metal electrode is applied.[98,106] Approaches to improve the perovskite/CE energy-level mismatch either aim at the heterogeneous incorporation of hole-extracting materials with a VBM lower than the CEs' WF[99,107] or at the modification of the perovskite's VBM at the perovskite/CE interface.[98,108]

The latter approach was adopted by Zhong and coworkers, post-treating a $CsPbI_2Br$ perovskite film surface with hexyltrimethylammonium bromide (HTAB), which decreased the energy offset between the perovskite and the CE from 0.70 eV in the pristine perovskite to 0.32 eV in the HTAB-treated one, as shown in **Figure 8**a.[98] This lowered energy mismatch increased the V_{OC} from 1.13 V for the pristine perovskite to 1.20 V for the HTAB-treated perovskite in C-PSCs. The HTAB-treated film additionally shows suppressed defect-induced charge carrier recombination and increased hydrophobicity, leading to devices that maintained 90% of their initial PCE over 330 h at 40–60% humidity and temperature of 85 °C. The HTAB-treated PSCs showed an average PCE of 13.9%. Chen et al. conducted a perovskite post-treatment on $MAPbI_3$ and $FAPbI_3$ (where MA is methylammonium and FA is formamidinium) using another long alkyl chain ammonium halide, namely, pentafluorophenylethylammonium iodide (F5PEAI), to create a passivating 2D perovskite phase at the perovskite/CE interface.[101] As shown in Figure 8b, they were able to increase the V_{OC} of their post-treated PSCs from 0.92 and 0.96 V for the nontreated PSCs to 0.98 V and 1.02 V for $MAPbI_3$ (PCE: 16.24%) and $FAPbI_3$ (PCE: 17.47%), respectively.

A similar approach was further adopted by Wu et al. to passivate a $MAPbI_3$ perovskite layer with phenethyl ammonium iodide (PEAI) that increased the films' hydrophobicity, smoothened the perovskite surface, increased the interface area, and lowered the defect concentration.[99] In combination with a copper phtalocyanine(CuPc)-modified CE, they were able to build PSCs with a maximum PCE of 13.41% that maintained 93% of their initial efficiency for 300 h (30% humidity, 70 °C). CuPc was integrated into the CE to lower the energy offset between the perovskite's VBM and the electrode's WF, while at the same time blocking the electron transfer from perovskite to electrode due the high-energy CBM of CuPc. In this direction, Liu and coworkers resorted to a CuPc modifier to increase the hole extraction from the perovskite to a CE but deposited it as a separate layer on top of $CsPbI_2Br$ perovskite film to build C-PSCs with a maximum PCE of 11.04%.[109] Gong et al. increased the VBM of $CsPbBr_3$ not by surface post-treatment but by adding small amounts of tetra-bisphenol A (TBBPA) in the bulk of the perovskite layer to enhance the hole extraction capability into the CE.[108] In addition, the TBBPA-treated perovskite was characterized by larger grain sizes and fewer trap states than the unmodified one, resulting in PSCs achieving a maximum efficiency of 9.82%.

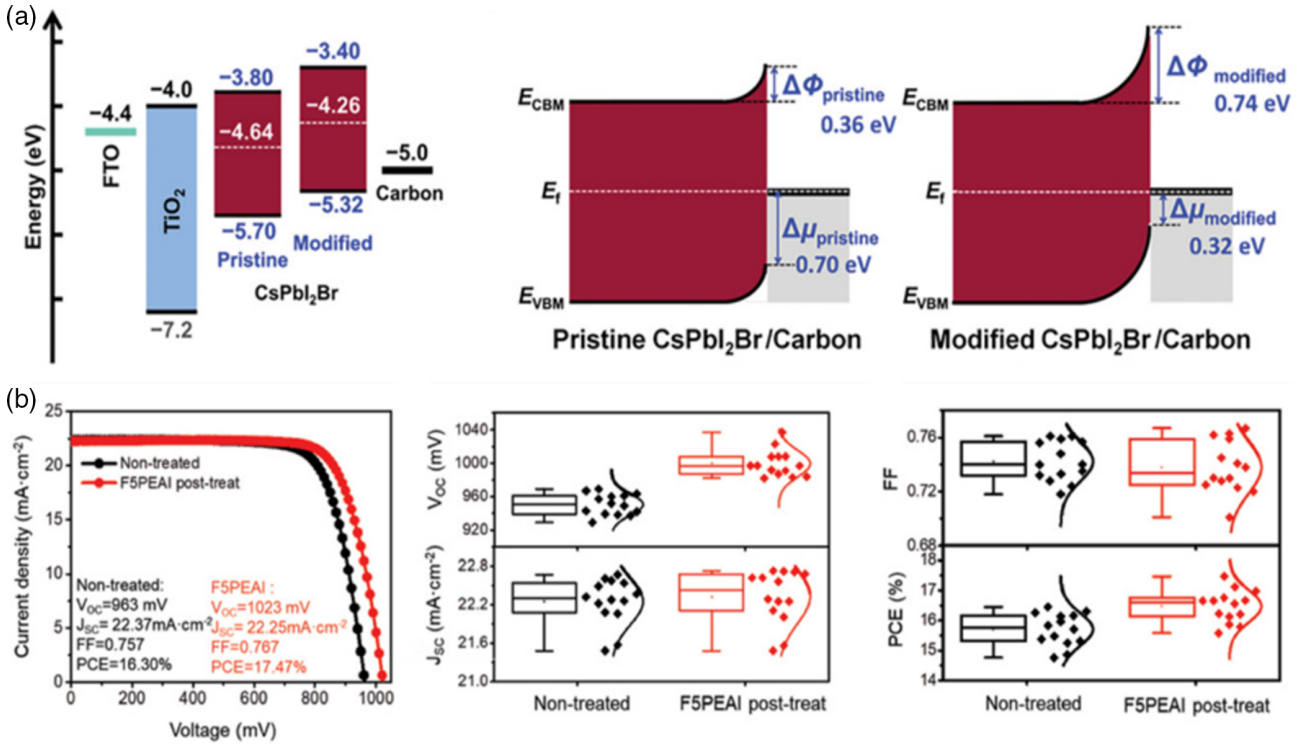

Figure 8. a) Energy diagram of a C-PSC incorporating a pristine $CsPbI_2$ photoactive layer in comparison with a HTAB-post-treated $CsPbI_2$ one. Adapted with permission.[98] Copyright 2021, Wiley-VCH. b) C-PSCs performances comparing pristine $FAPbI_3$ (black) and F5PEAI-post-treated $FAPbI_3$ (red) perovskite layers. Reproduced with permission.[101] Copyright 2021, Wiley-VCH.

The major goal of the previously discussed perovskite and CE modifications is to lower the energy mismatch at the perovskite/CE interface. In addition, these modifications are accompanied by enhanced optoelectronic properties, for example, reduced charge carrier recombination, which result in increased C-PSC performances. In contrast to those examples, Lin et al. suggested a new C-PSC device design that is based on the idea of a perovskite layer that is not entirely p or n doped due to PbI_2 or MAI excess, respectively, but consists of two separate parts, one of which is n doped while the other one is p doped.[106] A similar active-layer architecture creates a built-in field that encourages the charge separation and suppresses recombination. From their simulations, they concluded that an optimal $MAPbI_3$ perovskite layer would consist of a 400 nm-thick n-doped and a 700 nm-thick p-doped layer with doping concentrations of 10^{15} and 10^{19} cm^{-3}, respectively. An optimized C-PSC from such a perovskite layer could reach a theoretical PCE of 25.07%.

While the modified perovskite layers in C-PSCs are used to achieve a more efficient hole extraction that positively affects device PCEs, the efficiency-suppressing factors related to the suboptimal conductivity of CEs as well as their typically improvable small contact area with the perovskite photoactive layer are other issues that have to be seriously tackled. Chu et al. tried to face these bottlenecks by depositing a CE consisting of carbon black nanoparticles and carbon fibers (CFs) onto a $MAPbI_3$ perovskite layer to build a device that achieved a maximum PCE of 14.1% due to good conductivity and high perovskite/CE contact area.[100] In addition, they conducted a Mott–Schottky analysis and determined that nanosized noncontact areas do not hinder the hole extraction from the perovskite into the CE as they are overcome by a driving force of the built-in field originating from the band offset at the perovskite/electrode interface. In contrast, macrosized noncontact areas significantly suppress the hole extraction. The group of Huang improved the contact area using a mixture of CNTs and CFs as the CE to incorporate additional highly conductive pathways within this last one.[102] C-PSCs containing this electrode material and $MAPbI_3$ as the photoactive layer showed a maximum PCE of 11.80%, outperforming C-PSCs prepared with electrodes consisting of pure CNTs or CFs.

CEs can be prepared either through high-temperature or through low-temperature fabrication procedures (for a detailed review on the topic, we address the reader to very recent and complete reviews[110,111]). For the former fabrication approach, all layers of the solar cells except the perovskite ones are prepared in separate high-temperature steps and finally the temperature-sensitive photoactive perovskite is incorporated into a mesoporous buffer layer which separates the CE from the electron-transporting layer (see **Figure 9**).[112]

In contrast, low-temperature fabrication of the carbon back electrode allows to adopt a layer-by-layer method in which the CE can be deposited through different low-temperature procedures. In contrast to metal electrode deposition, which is an energy-demanding vacuum-assisted fabrication, those CE deposition methods are not only scalable for high-throughput industrial fabrication but, due to the low-temperature processability, they also require less energy to be processed and thereby are less cost intensive. In addition, the high abundancy of carbon (CEs have been derived from a variety of plants and biomasses [113–115]) lowers the production cost even further. Wu et al. demonstrated a procedure to not only deposit a dense carbon back electrode via electrospray printing but also to fabricate an entire solar cell using this method, as shown in **Figure 10**.[97] In comparison with doctor-bladed CEs, these electrosprayed CEs, consisting of a mixture of carbon black nanoparticles and graphite, showed a lower sheet resistance due to denser films and lower average carrier lifetimes, indicating faster hole extraction originating from an increased interfacial charge transfer. PSCs containing the electrosprayed electrodes showed a PCE of 14.41%, which was significantly higher than that of PSCs with doctor-bladed ones (11.14%). Furthermore, the possibility to fabricate entire C-PSCs through solution-based low-temperature processes opens up interesting perspectives for the manufacturing of flexible PSCs.[107,116,117] A preliminary example in this direction was reported recently by Que and coworkers, who built

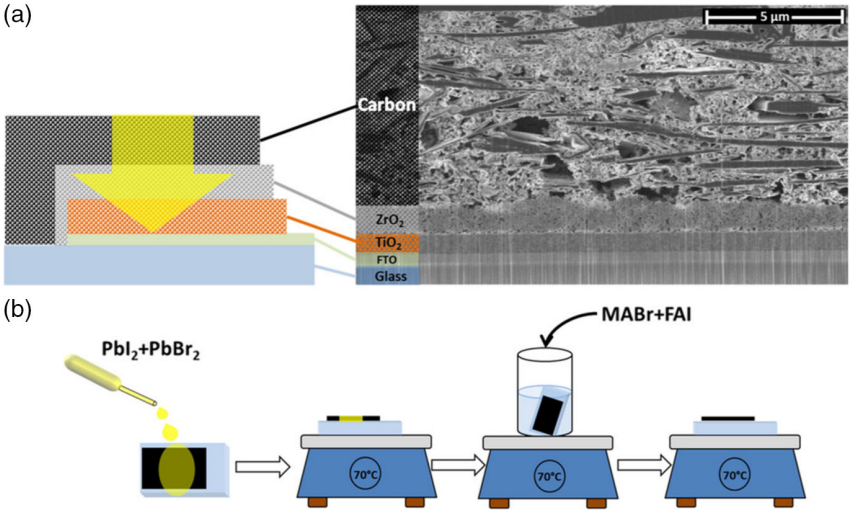

Figure 9. a) Sketch and SEM cross section of a high-temperature-fabricated C-PSC. The perovskite is incorporated through the porous layers as the last fabrication step, depicted by the yellow arrow in (a). b) Two-step perovskite deposition in which the porous layers of the cell are first soaked with PbI_2 and $PbBr_2$ solution and later the cell is dipped into a solution of MABr and FAI. Reproduced with permission.[112] Copyright 2021, Wiley-VCH.

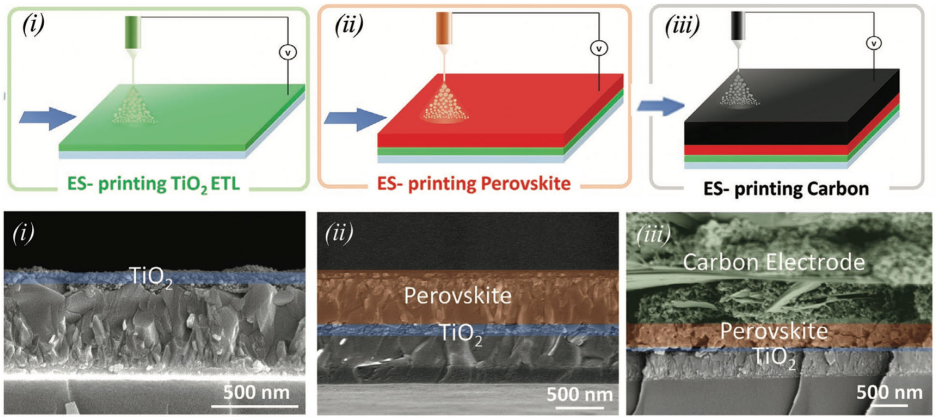

Figure 10. Layer-by-layer electrospray fabrication of entire C-PSCs. Reproduced with permission.[97] Copyright 2020, Wiley-VCH.

flexible $MAPbI_3$-based C-PSCs with doctor-bladed CEs on flexible polyethylene naphthalate/ITO substrates that showed a maximum PCE of 11.53% and retained 69% of their initial efficiency after 2000 bending cycles (2 mm bending radius).[118]

To construct well-performing large active area solar cells, Chen et al. chose a modular PSC architecture glass/FTO/SnO_2/$Cs_{0.05}(FA_{0.85}MA_{0.15})_{0.95}Pb(I_{0.85}Br_{0.15})_3$/CE as well as a glass/FTO/CE charge collector which they pressed onto the PSC by contacting both CEs.[105] This modular architecture enhanced the lateral conductivity of the back electrode and enabled the fabrication of 1 cm^2 active-area PSC with a maximum PCE of 11.2%. The authors also compared the performance of three CE materials like graphene, carbon nanocoils, and multiwalled CNTs (MWCNTs) and found that MWCNTs outperformed the other materials in terms of hole extraction ability, perovskite/CE band alignment, electrical conductivity, and thermal stability.

A different approach to deposit the CE is to prefabricate it and to then transfer it onto the PSC. For this procedure the contact of the perovskite/CE interface is increased by applying pressure on the cell. Such a preparation method was demonstrated by the group of Lee, who constructed a separate hybrid graphene/dry-spun CNT CE and then deposited it on the solar cell using a laminator.[104] Their $MAPbI_3$-based PSCs that incorporated also a Spiro-OMeTAD HTM showed a maximum PCE of 15.36% and maintained 86% of the initial PCE after 500 h (25 °C, 50% humidity) due to the presence of the highly hydrophobic CE. Teixeira et al. used separately fabricated transferable CEs to demonstrate a direct comparison of different electrodes on PSCs.[119] This was achieved by first fabricating and measuring PSCs with gold electrodes. Those electrodes were removed again, CEs were transferred onto that same PSCs, and finally the PSCs were measured with exchanged electrodes (the PSC incorporated the HTM Spiro-OMeTAD). The PSCs with CEs showed a maximum of 89% of the PCE that was obtained originally with the gold electrode.

It is important to mention that CEs are not only applied in high-performing lead-based PSCs but also in their lead-free counterparts in which the highly toxic Pb is substituted with less toxic metals. In general, lead-free PSCs achieve efficiencies that cannot be compared with those of the lead-based counterparts, and this results in relatively low PCEs also when CEs are introduced. Panneerselvam and Angaiah built lead-free C-PSCs based on $MASnI_3$ on which they deposited CEs that incorporated either Cu_2AgInS_4 (CAIS) or $Cu_2AgInSe_4$ (CAISe) nanoparticles to increase the CEs' hole extraction capability.[120] C-PSCs with the CAIS-modified CE achieved a PCE of 4.24% in comparison with 2.69% of C-PSCs that incorporated an unmodified CE. Another example of lead-free perovskite materials is the highly stable all-inorganic double-perovskite $Cs_2AgBiBr_6$ that was used as the photoactive layer by the group of Tang to prepare highly sustainable C-PSCs.[121] These solar cells showed a maximum PCE of 2.57% for Li^+-doped $Cs_2AgBiBr_6$, which is not far from the maximum efficiencies of around 3% obtained from analogous PSCs based on this material using metal electrodes.[122]

It is important to remind that there are also ways to fabricate HTM-free PSCs other than applying CEs. Song et al. showed such an example by replacing a CE with a screen-printed electrode consisting of indium tin oxide (ITO) nanoparticles.[123] Due to the increased light reflectance of ITO as well as its lower WF, which enhances hole extraction, tin-based PSCs' PCE can be increased from 5.4% when the ITO nanoparticle electrode is used in comparison with 3.0% with a CE.

5. Smart HTMs for PSCs

Up to now we have discussed the most recent opportunities offered by newly developed HTMs that can substitute Spiro-OMeTAD for the role of hole transporters without featuring the same instability problems related to the presence of the added dopants. As it is anyway also well recognized, to ensure PSC stability, it is necessary to delay or suppress any other decomposition pathway triggered by environmental factors such as, primarily, atmospheric humidity but also heat and excess irradiation. To cope with these second major issues, the incorporation of a protective function within the HTM, particularly for direct-architecture devices, can be considered a smart approach to overcome device instability. In addition, for both direct n–i–p and inverted p–i–n configurations, other aspects may become relevant, such as the effect of light on organic HTMs, thus calling for optically engineered species to improve overall performances, or solvent orthogonality issues, requiring the deposition of stable

redissolution layers. In this paragraph, we will extend the discussion to these aspects in relation to the design of novel "smart" HTMs and, for logistic reasons, we will start with examining the latter cases of optically engineered and solubility engineered HTM in PSCs.

The idea that photoexcited or electrically induced configurations of molecular or polymeric constituents of an organic HTM can have a huge impact in determining device performance has recently emerged. The formation of properly oriented electric dipole layers at the HTM/perovskite interface can result in improved charge extraction and reduced charge recombination, thus providing overall better PCEs. This concept was first explored by Hu and coworkers in 2016, reporting on the beneficial effect of photoinduced dipoles in thieno[3,4-b]thiophene-alt-benzodithiophene (PTB7) polymeric HTM on the performance of direct-architecture PSCs.[124] When compared with crystalline P3HT, the amorphous PTB7 was found to be able to undergo partial alignment of optically generated dipoles under the influence of the device's built-in potential. By carrying out magneto-photocurrent measurements under the influence of an external electric field, they proved that the presence of these dipoles partially suppresses the recombination of the photogenerated charge carriers in the bulk of the perovskite layer. Following this interesting concept, the group of Park engineered the optical features of HTM layer in a p–i–n PSC (where the HTM is the first layer to absorb the incoming light) by designing organic molecules that have a high transition dipole moment at the excited state and can be processed as an interlayer between NiO_x HTM and the perovskite absorber.[125] Their structures can undergo keto-enol tautomerism that causes an excited-state intramolecular proton transfer (ESIPT) process to take place after light absorption, as shown in **Figure 11**a. This transient structural variation is accompanied a change in dipole moment and polarizability, which can be further tuned by adding electron donor or acceptor moieties to the main molecular scaffold. By applying this concept, the authors achieved interesting results in terms of PCEs, with considerably reduced interfacial charge recombination in the resulting PSCs, as well as improved photostability due to the UV-blocking properties of the wisely engineered molecular HTMs. The same group also very recently reported an update to this strategy, by further developing the idea to achieve not only control over the excited-state polarizability of the HTMs but also over their aggregation properties, which drive charge transport in organic semiconductors-based layers.[126] The structure of the designed compounds is shown in Figure 11b, together with a scheme depicting the effect of the oriented excited-state dipoles within an inverted PSC architecture. The two molecules have a D–A character, with a triarylamine donor and an imidazole-based acceptor moiety. The second derivative (DNI) features an extended π-conjugation which favors intermolecular interactions in the solid state between adjacent molecules to boost aggregation and charge mobility, as demonstrated through grazing-incidence X-ray diffraction and hole mobility measurements. Overall, the synergy between the dipolar and aggregation effects led to improved charge extraction at the perovskite/HTM interface and prolonged stability of the devices kept in air at room temperature and under intense illumination. The generation of an electric dipole layer that increases the built-in potential in a PSC and thus causes the improvement of the overall performance can also be achieved by implementing smart doping of an organic HTM. A recent example reported by Kim and coworkers demonstrates the validity of this approach using a D–A-conducting polymer HTM with high doping capability by means of a tetrafluoro-tetracyanoquinodimethane (F4-TCNQ) interfacial dopant in direct-architecture PSC.[127] The establishment of the dipole layer and its entity was demonstrated by conducting Kelvin probe force microscopy measurements to track the WF variation, originating as a consequence of effective doping. The devices containing similar interfacial-doped HTMs provided better J_{SC} and FF compared with the un-doped reference, pointing out at increased hole extraction efficiency. In inverted PSC architectures, with generally lower efficiencies compared with direct ones, polymer-based HTMs such as PEDOT:PSS, PTAA, and Poly-TPD are widely used, either alone or in composite structures with other hole-extracting materials.[128–130] These HTMs result in good morphological properties and high efficiency, but inferior reproducibility and stability, in particular when dopants are needed for high-performance devices. As compared with polymer HTMs, small-molecular HTMs exhibit chemical structural tunability, design flexibility, and high purity. Unfortunately, their application in p–i–n configurations is hindered by their potential partial redissolution during the subsequent deposition of the perovskite layer from mixtures of highly polar solvents (DMF/DMSO). Even if this redissolution is sometimes minimal due to relatively good solvent orthogonality, it might be enough to diminish the HTM layer quality. A beneficial approach to improve the solvent stability of molecular HTMs used in inverted configurations is to resort to crosslinking strategies that can be activated once the HTM has been deposited, thus making it completely insoluble. In the past few years, some examples of this method have appeared in the literature, in which small-molecule HTMs were endowed with crosslinking ability, by conducting tailored modifications of their original structure with the introduction of a polymerizable functional group such as simple ethylene, as shown in **Figure 12**.[131–134] The effective crosslinking process can be then activated through different methods. In the first example reported by Hsu and coworkers, a *N,N′*-bis(tolyl)-*N,N′*-bis(vinylphenyl)-1,1′-biphenyl-4,4′-diamine (DVTPD) HTM was used, that can undergo simple thermally induced crosslinking of the styryl groups at 180 °C (Figure 12a), forming a robust film on top of a VO_2 electron blocking layer.[131] With this highly stabilized HTM structure and a top electron transporting layer (ETL) based on an ionic fullerene, they achieved maximum PCE of 18.8% and prolonged device stability in high humidity conditions. In another similar case, Getautis and coworkers reported on the use of cost-effective enamine-based cross-linkable HTMs, as the one shown in Figure 12c, in p–i–n PSC configuration, achieving a promising PCE of 18.14%.[133] Here, the crosslinking process was thermally initiated at 231 °C, which was identified after conducting an accurate thermal characterization of the newly synthesized HTM through differential scanning calorimetry and thermogravimetric analysis. Tremblay et al. designed a photocrosslinkable HTM based on a bis(triarylamine) molecule bearing cinnamate side chains[132]: photocrosslinking is a potentially more advantageous process with respect to thermally induced crosslinking, as it does not require high temperature (>150 °C) and thus can be conducted at ambient temperature also on plastic substrates.

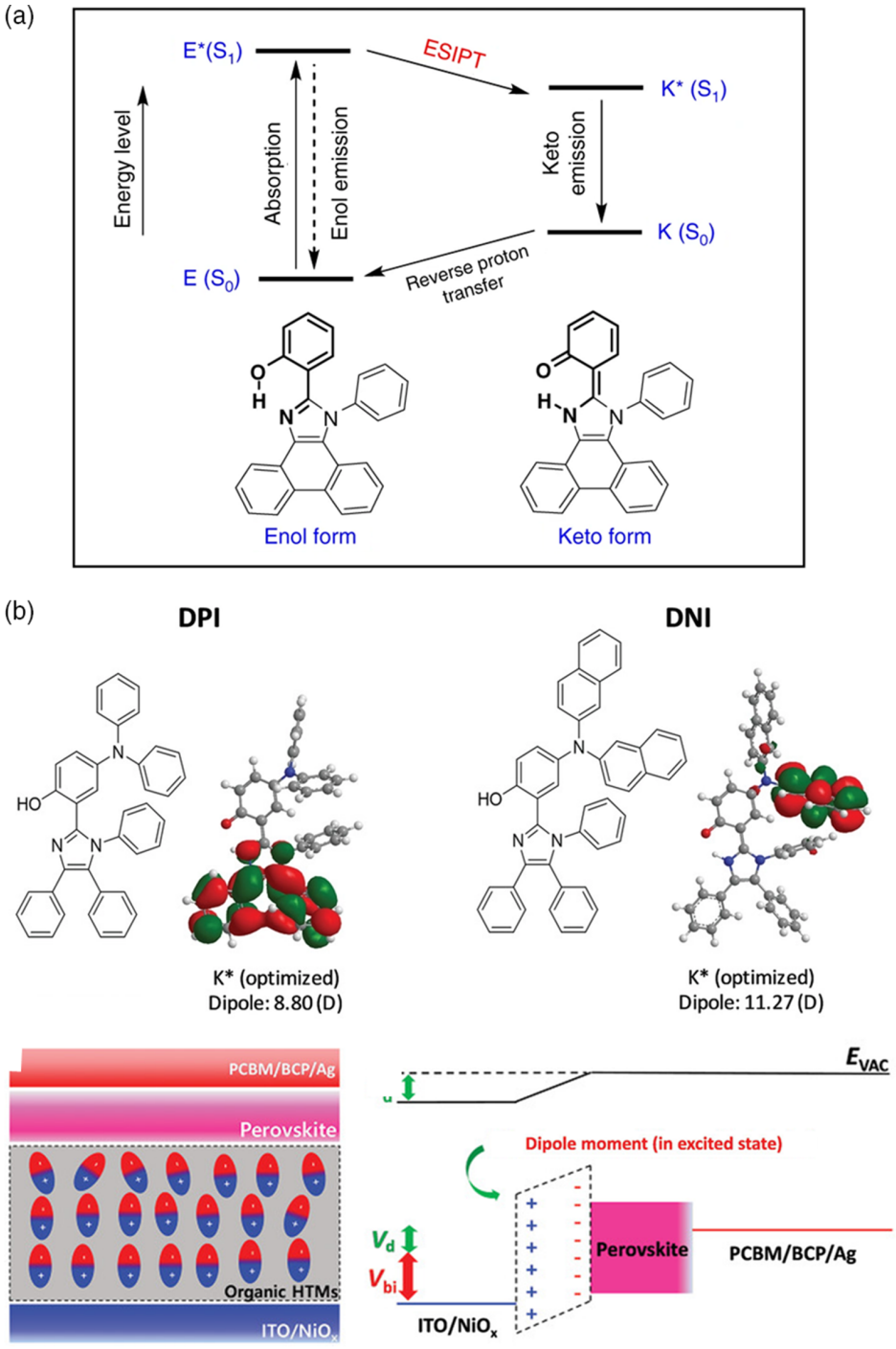

Figure 11. Emerging smart molecular HTMs for optically engineered hole extraction layers in PSCs. a) Basic molecular structure of these HTMs with illustration of the ESIPT process that drives the change in excited-state dipole moment. Reproduced under the terms of the Creative Commons CC BY License.[125] Copyright 2018, The Author(s). Published by Springer Nature. b) D-A structures with improved excited-state dipole moment and solid-state self-aggregation properties. Adapted with permission.[126] Copyright 2020, Wiley-VCH.

With a similar approach, the authors achieved a stable, dopant-free HTM, whose performance in inverted PSCs was found to be perfectly comparable with that achieved using a doped poly-TPD HTM.

Crosslinkable HTMs can also be considered valuable alternatives for direct-architecture n–i–p PSCs, being based on 3D network structures where a high density of charge-transport channels can be achieved, together with good thermal and

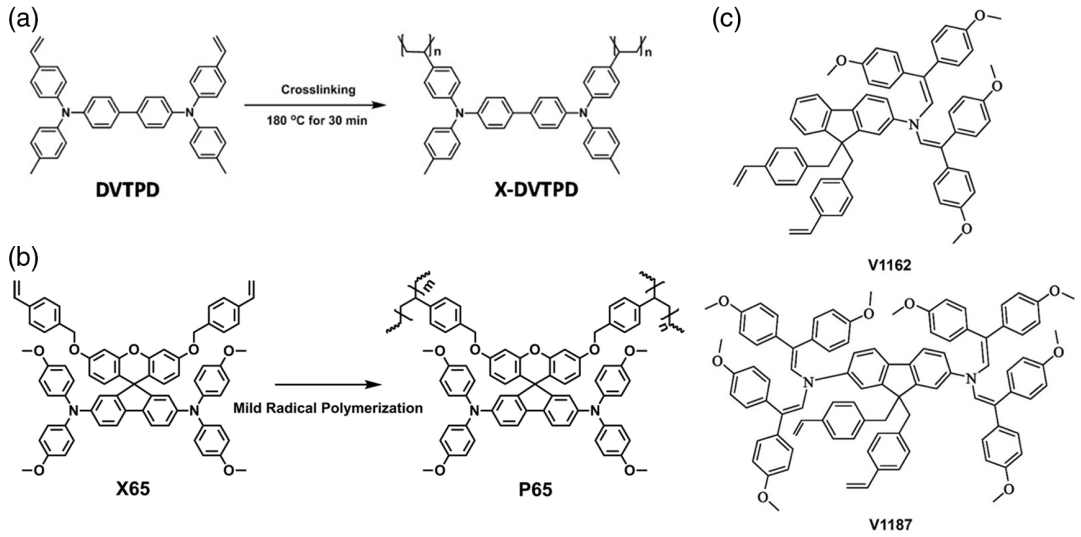

Figure 12. Examples of crosslinkable small-molecule HTMs for PSCs. a) A thermally crosslinkable *N,N′*-bis(tolyl)-*N,N′*-bis(vinylphenyl)-1,1′-biphenyl-4,4′-diamine (DVTPD) HTM used in an inverted PSC. Reproduced with permission.[131] Copyright 2018, American Chemical Society. b) A spiro[fluorene-9,9′-xanthene]-3′,6′-diol-based, crosslinked polymer, obtained through a mild free-radical polymerization as a dopant-free HTM for n–i–p-type PSCs. Reproduced under the terms of the Creative Commons CC BY License.[134] Copyright 2020, The Authors. Published by ELSEVIER B.V. and Science Press. c) Molecular structures of two enamine-based crosslinkable HTMs used in p–i–n devices. Reproduced with permission.[133] Copyright 2020, Wiley-VCH.

mechanical durability. In this regard, Sun and coworkers recently reported on the use of a novel spiro[fluorene-9,9′-xanthene]-3′,6′-diol-based crosslinked polymer (Figure 12b), obtained through mild free-radical polymerization as a dopant-free HTM for n–i–p-type PSCs.[134] With a similar HTM they achieved PCEs slightly lower than those obtained with a classically doped Spiro-based HTM (17.7% vs 19%) but a remarkably higher stability in high-humidity conditions, most likely ensured by the improved hydrophobicity of the layer following crosslinking.

Other remarkable crosslinking approaches reported in the past two years by different groups regard the incorporation of fluorine moieties within a crosslinkable and dopant-free small-molecule HTM to further boost hydrophobicity of the charge-extracting layer and target defect-passivating interactions with the perovskite surface,[135] the use of electropolymerization to induce in situ formation of polyamine-based dopant-free HTMs for inverted PSCs,[136] and the in situ thermal conversion of solution-processable xanthate precursors into the corresponding insoluble glycol-derivatized poly(1,4-phenylenevinylene) HTMs with different hydrophilicity profiles influencing final device performance.[137]

The insertion of an interfacial layer between the perovskite and the HTM or the HTM and the top metal electrode has been shown in other cases to be advantageous for reducing charge recombination in PSCs,[138,139] also through the passivation of surface defects in the semiconductor.[140–142] Engineering of the perovskite/HTM interface at the molecular level has even allowed Seo and coworkers to achieve outstanding PSC performance (a PCE of 22.7%) and stability, using a pristine, undoped P3HT HTM,[143] which normally provides relatively low PCEs (10–15%,[39,144] slightly better ones if doped[145,146]). The concomitant perovskite surface passivation with a quasi-2D perovskite layer and the supramolecular hydrophobic interaction of this last one with the lateral chains of the P3HT HTM created the right conditions to form a highly oriented, self-assembled semiconducting polymer layer with very high hole mobility. If the passivation layer is based on a highly hydrophobic material, further protection from humidity-driven decomposition can be achieved.[147] This was the case, for example, in the work of Chaudhary et al.,[148] where a solution-processable poly (4-vinylpyridine) film was used to passivate the perovskite surface, through the coordination of the pyridine moieties to undercoordinated lead atoms on the surface of the perovskite light absorber. Similarly, Prabakar and coworkers used two highly hydrophobic, dopant-free, donor–π–acceptor semiconducting polymer HTMs containing thiophene residues, able to passivate surface defects on the perovskite photoactive layer and to fabricate standard-architecture PSCs with good efficiency and environmental stability.[149]

A notable emerging direction in the field of smart HTM development that deserves to be reminded in this Review is undoubtedly the implementation of self-assembled monolayers (SAMs) at the interface between the HTM itself and the perovskite layer in inverted PSCs, similarly as it was done in the past for electron-transporting layers in direct-architecture devices.[150] The first example of a SAM HTM implemented in a p–i–n PSC was reported in 2018 by the groups of Getautis and Albrecht using a dopant-free small-molecule HTM functionalized with phosphonic groups able to directly bind to the transparent conductive oxide (TCO) surface.[151] More recent reports have described the use of carboxylic acid-decorated species for anchoring to the TCO,[152] as well as the systematic study of the effect of different anchoring groups on the final device PCE and stability.[153] However, the most remarkable achievement of a similar strategy is the incorporation into tandem solar cells, allowing

considerable simplification and high versatility of device architecture design: with the SAM HTM approach indeed, Albrecht and coworkers were able to fabricate both CIGSe/perovskite[154] and silicon/perovskite monolithic solar cells[155] with very high efficiencies and environmental stability. As discussed along this entire Review, the improvement of hydrophobicity at the level of the HTM has often provided good opportunities to obtain PSCs with interesting stability profiles with respect to the exposure to ambient moisture or even to excess humidity. In contrast, it is necessary to highlight here that hydrophobic materials/additives/functional groups are only a "passive" way to hinder the income of water molecules across a PSC, so as to avoid their contact with the highly water-sensitive photoactive perovskite layer. Similar hydrophobic HTMs might be therefore able to ensure such a blocking effect only until they do not start to degrade themselves, thus not being anymore able to act as a barrier for humidity. A different perspective could be offered by the development of HTMs that have the capability of "actively" transforming water into unharmful or even beneficial species, which ultimately boost the overall PSC performance. In this regard, some of us have recently reported on the incorporation of a water-splitting active layer as the HTM in n–i–p PSCs.[156] Endowing an HTM with water oxidation and reduction properties is indeed a very peculiar and potentially disruptive approach to solve the problem of water-driven perovskite decomposition, which might even lead to the realization of compact photovoltaic technologies able to generate at the same time both electricity and hydrogen as a solar fuel. Our proof-of-concept water-splitting active HTM was realized by incorporating CuSCN nanoplatelets (CuSCN-NPs, a transmission electron microscopy (TEM) image is shown in **Figure 13**a, together with an estimation of the average diameter obtained through dynamic light scattering, DLS) into P3HT matrix, producing a nanocomposite in which both the components have hole-transport properties. In this blend, a hole transfer process between the inorganic nanofillers and the semiconducting polymer host is detected through ESR spectroscopy (here the signal of the P3HT polaron is considerably increased in the presence of the blended CuSCN-NPs, see Figure 13b). The ability to conduct both water oxidation (at the composite valence band) and reduction (at the CuSCN Fermi level) was demonstrated by conducting electrochemical studies on the CuSCN@P3HT composite and by comparing

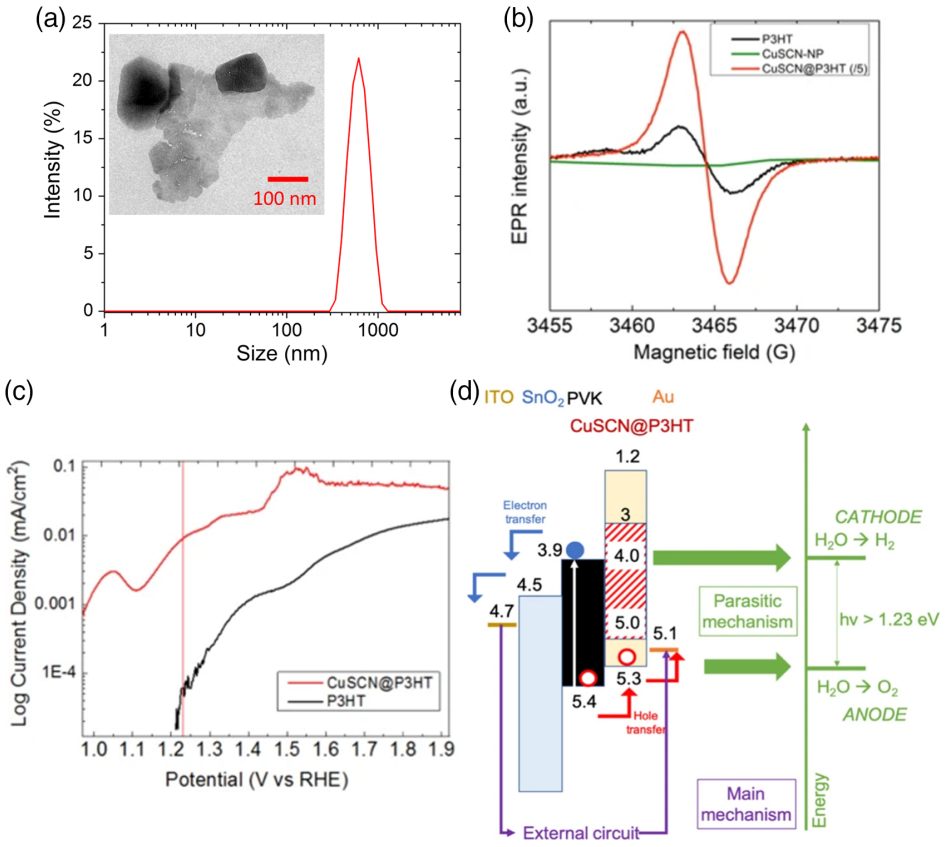

Figure 13. A water-splitting "active" CuSCN@P3HT composite HTM transforms harmful water molecules into hydrogen and oxygen. This last one further promotes the in situ p-doping of P3HT, improving the charge transport properties of the layer during PSC operation in high-humidity conditions. a) CuSCN-NPs used as nanofillers for a P3HT HTM matrix (TEM image and DLS spectrum). b) ESR spectra of the composite HTM, highlighting the considerably greater polaronic response of P3HT in the presence of the inorganic nanofillers. c) Linear sweep voltammetry curves (anodic region) of the CuSCN@P3HT composite HTM and neat P3HT, highlighting the current contribution of the two different materials at 1.23 V. d) Working mechanism of a water-splitting HTM-endowed direct-architecture PSC, in which the parasitic mechanism occurring within the HTM itself promotes the generation of both hydrogen and oxygen molecules from incoming moisture. Reproduced under the terms of the Creative Commons CC BY 4.0 License.[156] Copyright 2021, The Authors. Published by Springer Nature.

them with results obtained on pristine P3HT: in Figure 13c, the anodic regime is shown, where a remarkable difference in current response between the composite and the neat P3HT film is well visible at 1.23 V, the minimal potential required to promote water oxidation. Also, at the cathodic side (not shown), a clear contribution to water reduction in the presence of CuSCN was detected. The additional peculiarity of a similar "active" HTM resides in the fact that the in situ-generated oxygen molecules can act as p-dopants for the P3HT phase (as shown through Kelvin probe experiments in which an evident downshifting of the WF is found), improving the charge transport properties of this last one during device operation in RH > 80%: it was indeed in such conditions and not in "dry" ones that the potential of this water-splitting active HTM was revealed, allowing to achieve a stable (and even slightly improved) PCE in standard PSCs over a 1 month time storage in a water-saturated atmosphere. In Figure 13d, the occurrence of a water-splitting process within the HTM is conjectured to make use of a part of the photocurrent generated by the solar cell (through the there-defined "main mechanism") to install a "parasitic mechanism" able to promote the generation of oxygen and hydrogen molecules, being the right energetics for both reactions available within the layer itself.

6. Conclusions and Outlook

Within this contribution, we wanted to highlight new scenarios in the development and application of smart HTMs for PSCs. We started from an experimental and highly validated evidence that supports the closing of the first PSC era, represented by high-performance devices with a limited shelf-life and reflecting the impossibility of producing commercial items exploiting the very popular Spiro-based HTM, whose golden age appears to have reached a definitive end. For this reason, researchers have learnt how to resort to new inorganic and organic HTMs, by exalting their noninnocent role to guarantee similar peak performances of Spiro-based devices that also prolong long-term stability, thus closing the gap for industrial scale-up. Within this scenario, we believe that a species like CuSCN will become the new main character of upcoming PSC research, thanks to its chemical stability in high humidity conditions and its optimal electronic properties. However, there are some issues in the processing as the solubility in sulfide was demonstrated to be a problem for the underneath perovskite layer, so that miniaturization (as done in our P3HT-CuSCN composite HTM work[156]) can perhaps fix this issue. In addition, the inspiration of the experienced organic chemists will help the community in the development of new molecules able to replace Spiro at lower costs of production and without the need for additional dopants. These new small molecules are already under development and are characterized by an extremely sophisticated structural design and highly optimized electronic properties. Finally, there is the possibility of completely cutting the HTM layer, thus notably simplifying device architectures, by resorting to the so-called HTM-free C-PSCSs, that use CEs having both the quality of hole acceptors and real top electrodes. Apart for the essential benefit in terms of economic savings that results from the elimination of the highly expensive gold electrode, the use of carbon-based layers can improve PSC stability and, after proper interface engineering with the perovskite layer, can open perspectives for application in tandem solar cells, devices in which the number of layers is undoubtedly an issue to be tightly monitored.[157] In addition, drastic cost reduction paves the way to new opportunities for similar ultracheap photovoltaic technologies, such as the ever-growing need for viable power sources to be applied in the internet of things (IoT) field.

All these intriguing possibilities require versatile and reproducible processing that actual lab-scale methodology does not allow. For this reason, there is the need of exploring new and even not yet considered approaches for thin-film photovoltaics production, such as for instance spray coating[158] and sputtering,[159] that can overcome, in principle, the intrinsic limitation of CuSCN processing, opening the way for the new (and ultimate) era of PSC development: the industrialization.

Acknowledgements

T.G. acknowledges the financial support of the European Commission through the H2020 FET-PROACTIVE-EIC-07-2020 project LIGHT-CAP (no. 101017821), of the Deutsche Forschungsgemeinschaft (DFG) (project GA 3052/1-1) and Fonds der Chemischen Industrie (Verband der Chemischen Industrie e.V.). F.S. and T.G. further thank the DFG for the RTG 2204 "Substitute materials for sustainable energy technologies." Z.H. acknowledges support from the National Natural Science Foundation of China (NSFC) (nos. 61775091 and U2001216), Science, Technology and Innovation Commission of Shenzhen Municipality (no. JCYJ20180504165851864), and the Shenzhen Key Laboratory Project (no. ZDSYS201602261933302). F.L. acknowledges "Centro Levi Cases" of University of Padova for financial support (AMONRA project).

Open Access Funding provided by Universita degli Studi di Padova within the CRUI-CARE Agreement.

Conflict of Interest

The authors declare no conflict of interest.

Keywords

dopant-free hole-transporting materials, hole-transporting materials, inorganic materials, perovskite solar cells, smart materials

Received: July 8, 2021
Revised: August 2, 2021
Published online: August 19, 2021

[1] M. Jeong, I. W. Choi, E. M. Go, Y. Cho, M. Kim, B. Lee, S. Jeong, Y. Jo, H. W. Choi, J. Lee, J.-H. Bae, S. K. Kwak, D. S. Kim, C. Yang, *Science (80-.).* **2020**, *369*, 1615.
[2] Z. Hawash, L. K. Ono, Y. Qi, *Adv. Mater. Interfaces* **2018**, *5*, 1700623.
[3] E. Kasparavicius, A. Magomedov, T. Malinauskas, V. Getautis, *Chem. – A Eur. J.* **2018**, *24*, 9910.
[4] L. Hajikhanmirzaei, H. Shahroosvand, B. Pashaei, G. D. Monache, M. K. Nazeeruddin, M. Pilkington, *J. Mater. Chem. C* **2020**, *8*, 6221.
[5] A. T. Murray, J. M. Frost, C. H. Hendon, C. D. Molloy, D. R. Carbery, A. Walsh, *Chem. Commun.* **2015**, *51*, 8935.
[6] L. Calió, S. Kazim, M. Grätzel, S. Ahmad, *Angew. Chem., Int. Ed.* **2016**, *55*, 14522.

[7] J. H. Noh, N. J. Jeon, Y. C. Choi, M. K. Nazeeruddin, M. Grätzel, S. Il Seok, *J. Mater. Chem. A* **2013**, *1*, 11842.
[8] Z. Hawash, L. K. Ono, Y. Qi, *Adv. Mater. Interfaces* **2018**, *5*, 1700623.
[9] W. Han, G. Ren, J. Liu, Z. Li, H. Bao, C. Liu, W. Guo, *ACS Appl. Mater. Interfaces* **2020**, *12*, 49297.
[10] W. S. Yang, J. H. Noh, N. J. Jeon, Y. C. Kim, S. Ryu, J. Seo, S. I. Seok, *Science (80-.).* **2015**, *348*, 1234.
[11] Y. Deng, X. Zheng, Y. Bai, Q. Wang, J. Zhao, J. Huang, *Nat. Energy* **2018**, *3*, 560.
[12] D. Yang, T. Sano, Y. Yaguchi, H. Sun, H. Sasabe, J. Kido, *Adv. Funct. Mater.* **2019**, *29*, 1807556.
[13] G. Grancini, C. Roldán-Carmona, I. Zimmermann, E. Mosconi, X. Lee, D. Martineau, S. Narbey, F. Oswald, F. De Angelis, M. Graetzel, M. K. Nazeeruddin, *Nat. Commun.* **2017**, *8*, 15684.
[14] J. W. Jung, C.-C. Chueh, A. K.-Y. Jen, *Adv. Mater.* **2015**, *27*, 7874.
[15] M. Huangfu, Y. Shen, G. Zhu, K. Xu, M. Cao, F. Gu, L. Wang, *Appl. Surf. Sci.* **2015**, *357*, 2234.
[16] W. Sun, Y. Li, S. Ye, H. Rao, W. Yan, H. Peng, Y. Li, Z. Liu, S. Wang, Z. Chen, L. Xiao, Z. Bian, C. Huang, *Nanoscale* **2016**, *8*, 10806.
[17] H. Peng, W. Sun, Y. Li, S. Ye, H. Rao, W. Yan, H. Zhou, Z. Bian, C. Huang, *Nano Res.* **2016**, *9*, 2960.
[18] H. Sung, N. Ahn, M. S. Jang, J.-K. Lee, H. Yoon, N.-G. Park, M. Choi, *Adv. Energy Mater.* **2016**, *6*, 1501873.
[19] E. Singh, K. S. Kim, G. Y. Yeom, H. S. Nalwa, *ACS Appl. Mater. Interfaces* **2017**, *9*, 3223.
[20] N. Arora, M. I. Dar, A. Hinderhofer, N. Pellet, F. Schreiber, S. M. Zakeeruddin, M. Grätzel, *Science (80-.).* **2017**, *358*, 768.
[21] R. S. Sanchez, E. Mas-Marza, *Sol. Energy Mater. Sol. Cells* **2016**, *158*, 189.
[22] A. Di Carlo, F. Matteocci, S. Razza, M. Mincuzzi, F. Di Giacomo, S. Casaluci, D. Gentilini, T. M. Brown, A. Reale, F. Brunetti, A. D'Epifanio, S. Licoccia, in *14th IEEE Int. Conf. Nanotechnology*, IEEE, Piscataway, NJ **2014**, pp. 70–74.
[23] F. Lamberti, T. Gatti, E. Cescon, R. Sorrentino, A. Rizzo, E. Menna, G. Meneghesso, M. Meneghetti, A. Petrozza, L. Franco, *Chem* **2019**, *5*, 1806.
[24] A. Abate, D. J. Hollman, J. Teuscher, S. Pathak, R. Avolio, G. D'Errico, G. Vitiello, S. Fantacci, H. J. Snaith, *J. Am. Chem. Soc.* **2013**, *135*, 13538.
[25] G. Ren, W. Han, Y. Deng, W. Wu, Z. Li, J. Guo, H. Bao, C. Liu, W. Guo, *J. Mater. Chem. A* **2021**, *9*, 4589.
[26] A. Magomedov, E. Kasparavičius, K. Rakstys, S. Paek, N. Gasilova, K. Genevičius, G. Juška, T. Malinauskas, M. K. Nazeeruddin, V. Getautis, *J. Mater. Chem. C* **2018**, *6*, 8874.
[27] F. Lamberti, T. Gatti, E. Cescon, R. Sorrentino, A. Rizzo, E. Menna, G. Meneghesso, M. Meneghetti, A. Petrozza, L. Franco, *Chem* **2019**, *5*, 1806.
[28] X. Yin, Z. Song, Z. Li, W. Tang, *Energy Environ. Sci.* **2020**, *13*, 4057.
[29] K. Rakstys, C. Igci, M. K. Nazeeruddin, *Chem. Sci.* **2019**, *10*, 6748.
[30] Y. Wang, W. Chen, L. Wang, B. Tu, T. Chen, B. Liu, K. Yang, C. W. Koh, X. Zhang, H. Sun, G. Chen, X. Feng, H. Y. Woo, A. B. Djurišić, Z. He, X. Guo, *Adv. Mater.* **2019**, *31*, 1902781.
[31] W. Chen, Y. Wang, B. Liu, Y. Gao, Z. Wu, Y. Shi, Y. Tang, K. Yang, Y. Zhang, W. Sun, X. Feng, F. Laquai, H. Y. Woo, A. B. Djurišić, X. Guo, Z. He, *Sci. China Chem.* **2021**, *64*, 41.
[32] M. K. Nazeeruddin, C. Liu, C. Igci, Y. Yang, O. A. Syzgantseva, M. A. Syzgantseva, K. Rakstys, H. Kanda, N. Shibayama, B. Ding, X. Zhang, V. Jankauskas, Y. Ding, S. Dai, P. Dyson, *Angew. Chem., Int. Ed.* **2021**, https://doi.org/10.1002/anie.202107774.
[33] K. Rakstys, S. Paek, P. Gao, P. Gratia, T. Marszalek, G. Grancini, K. T. Cho, K. Genevicius, V. Jankauskas, W. Pisula, M. K. Nazeeruddin, *J. Mater. Chem. A* **2017**, *5*, 7811.
[34] Q. Fu, Z. Xu, X. Tang, T. Liu, X. Dong, X. Zhang, N. Zheng, Z. Xie, Y. Liu, *ACS Energy Lett.* **2021**, *6*, 1521.
[35] C. Igci, S. Paek, K. Rakstys, H. Kanda, N. Shibayama, V. Jankauskas, C. Roldán-Carmona, H. Kim, A. M. Asiri, M. K. Nazeeruddin, *Sol. RRL* **2020**, *4*, 2000173.
[36] J. Wang, X. Wu, Y. Liu, T. Qin, K. Zhang, N. Li, J. Zhao, R. Ye, Z. Fan, Z. Chi, Z. Zhu, *Adv. Energy Mater.* **2021**, 2100967.
[37] J. Yuan, Y. Chen, X. Liu, S. Xue, *ACS Appl. Energy Mater.* **2021**, *4*, 5756.
[38] M. Cai, V. T. Tiong, T. Hreid, J. Bell, H. Wang, *J. Mater. Chem. A* **2015**, *3*, 2784.
[39] T. Gatti, S. Casaluci, M. Prato, M. Salerno, F. Di Stasio, A. Ansaldo, E. Menna, A. Di Carlo, F. Bonaccorso, *Adv. Funct. Mater.* **2016**, *26*, https://doi.org/10.1002/adfm.201602803.
[40] T. Gatti, F. Lamberti, P. Topolovsek, M. Abdu-Aguye, R. Sorrentino, L. Perino, M. Salerno, L. Girardi, C. Marega, G. A. Rizzi, M. A. Loi, A. Petrozza, E. Menna, *Sol. RRL* **2018**, *2*, 1800013.
[41] Q. Hu, E. Rezaee, Q. Dong, H. Shan, Q. Chen, L. Wang, B. Liu, J.-H. Pan, Z.-X. Xu, *Sol. RRL* **2019**, *3*, 1800264.
[42] Q. Hu, E. Rezaee, M. Li, Q. Chen, C. Li, S. Cai, H. Shan, Z.-X. Xu, *Sol. RRL* **2020**, *4*, 1900340.
[43] J. Wang, Q. Hu, M. Li, H. Shan, Y. Feng, Z.-X. Xu, *Sol. RRL* **2020**, *4*, 2000109.
[44] Y. Liu, B. He, J. Duan, Y. Zhao, Y. Ding, M. Tang, H. Chen, Q. Tang, *J. Mater. Chem. A* **2019**, *7*, 12635.
[45] J. Peng, D. Walter, Y. Ren, M. Tebyetekerwa, Y. Wu, T. Duong, Q. Lin, J. Li, T. Lu, M. A. Mahmud, O. L. C. Lem, S. Zhao, W. Liu, Y. Liu, H. Shen, L. Li, F. Kremer, H. T. Nguyen, D.-Y. Choi, K. J. Weber, K. R. Catchpole, T. P. White, *Science (80-.).* **2021**, *371*, 390.
[46] J.-M. Wang, Z.-K. Wang, M. Li, K.-H. Hu, Y.-G. Yang, Y. Hu, X.-Y. Gao, L.-S. Liao, *ACS Appl. Mater. Interfaces* **2017**, *9*, 13240.
[47] J. Chen, N.-G. Park, *J. Phys. Chem. C* **2018**, *122*, 14039.
[48] R. Singh, P. K. Singh, B. Bhattacharya, H.-W. Rhee, *Appl. Mater. Today* **2019**, *14*, 175.
[49] L. C. Palilis, M. Vasilopoulou, A. Verykios, A. Soultati, E. Polydorou, P. Argitis, D. Davazoglou, A. R. bin Mohd Yusoff, M. K. Nazeeruddin, *Adv. Energy Mater.* **2020**, *10*, 2000910.
[50] Y. Hou, X. Du, S. Scheiner, D. P. McMeekin, Z. Wang, N. Li, M. S. Killian, H. Chen, M. Richter, I. Levchuk, N. Schrenker, E. Spiecker, T. Stubhan, N. A. Luechinger, A. Hirsch, P. Schmuki, H.-P. Steinrück, R. H. Fink, M. Halik, H. J. Snaith, C. J. Brabec, *Science (80-.).* **2017**, *358*, 1192.
[51] L. C. Palilis, M. Vasilopoulou, A. Verykios, A. Soultati, E. Polydorou, P. Argitis, D. Davazoglou, A. R. bin Mohd Yusoff, M. K. Nazeeruddin, *Adv. Energy Mater.* **2020**, *10*, 2000910.
[52] V. Sugathan, E. John, K. Sudhakar, *Renew. Sustain. Energy Rev.* **2015**, *52*, 54.
[53] T. Gatti, F. Lamberti, R. Mazzaro, I. Kriegel, D. Schlettwein, F. Enrichi, N. Lago, E. Di Maria, G. Meneghesso, A. Vomiero, S. Gross, *Adv. Energy Mater.* **2021**, 2101041.
[54] T. Gatti, F. Lamberti, R. Mazzaro, I. Kriegel, D. Schlettwein, F. Enrichi, N. Lago, E. Di Maria, G. Meneghesso, A. Vomiero, S. Gross, *Adv. Energy Mater.* **2021**, 2101041.
[55] P. Dalle Feste, M. Crisci, F. Barbon, F. Tajoli, M. Salerno, F. Drago, M. Prato, S. Gross, T. Gatti, F. Lamberti, *Appl. Sci.* **2021**, *11*, 2016.
[56] B. A. Nejand, V. Ahmadi, S. Gharibzadeh, H. R. Shahverdi, *ChemSusChem* **2016**, *9*, 302.
[57] P. Wang, J. Zhang, Z. Zeng, R. Chen, X. Huang, L. Wang, J. Xu, Z. Hu, Y. Zhu, *J. Mater. Chem. C* **2016**, *4*, 9003.
[58] N. Yamada, R. Ino, H. Tomura, Y. Kondo, Y. Ninomiya, *Adv. Electron. Mater.* **2017**, *3*, 1700298.
[59] J. A. Christians, R. C. M. Fung, P. V. Kamat, *J. Am. Chem. Soc.* **2014**, *136*, 758.

[60] S. Ye, H. Rao, Z. Zhao, L. Zhang, H. Bao, W. Sun, Y. Li, F. Gu, J. Wang, Z. Liu, Z. Bian, C. Huang, *J. Am. Chem. Soc.* **2017**, *139*, 7504.
[61] F. Matebese, R. Taziwa, D. Mutukwa, *Materials (Basel)*. **2018**, *11*, 2592.
[62] J. E. Jaffe, T. C. Kaspar, T. C. Droubay, T. Varga, M. E. Bowden, G. J. Exarhos, *J. Phys. Chem. C* **2010**, *114*, 9111.
[63] N. Wijeyasinghe, A. Regoutz, F. Eisner, T. Du, L. Tsetseris, Y.-H. Lin, H. Faber, P. Pattanasattayavong, J. Li, F. Yan, M. A. McLachlan, D. J. Payne, M. Heeney, T. D. Anthopoulos, *Adv. Funct. Mater.* **2017**, *27*, 1701818.
[64] N. Arora, M. I. Dar, A. Hinderhofer, N. Pellet, F. Schreiber, S. M. Zakeeruddin, M. Grätzel, *Science (80-.)*. **2017**, *358*, 768.
[65] I. S. Yang, S. Lee, J. Choi, M. T. Jung, J. Kim, W. I. Lee, *J. Mater. Chem. A* **2019**, *7*, 6028.
[66] C. Liu, L. Zhang, Y. Li, X. Zhou, S. She, X. Wang, Y. Tian, A. K. Y. Jen, B. Xu, *Adv. Funct. Mater.* **2020**, *30*, 1908462.
[67] T. Duong, J. Peng, D. Walter, J. Xiang, H. Shen, D. Chugh, M. Lockrey, D. Zhong, J. Li, K. Weber, T. P. White, K. R. Catchpole, *ACS Energy Lett.* **2018**, *3*, 2441.
[68] M. Tyagi, M. Tomar, V. Gupta, *Anal. Chim. Acta* **2012**, *726*, 93.
[69] N. M. Hosny, *Polyhedron* **2011**, *30*, 470.
[70] W. Chen, F.-Z. Liu, X.-Y. Feng, A. B. Djurišić, W. K. Chan, Z.-B. He, *Adv. Energy Mater.* **2017**, *7*, 1700722.
[71] F. Xie, C.-C. Chen, Y. Wu, X. Li, M. Cai, X. Liu, X. Yang, L. Han, *Energy Environ. Sci.* **2017**, *10*, 1942.
[72] S. Yue, K. Liu, R. Xu, M. Li, M. Azam, K. Ren, J. Liu, Y. Sun, Z. Wang, D. Cao, X. Yan, S. Qu, Y. Lei, Z. Wang, *Energy Environ. Sci.* **2017**, *10*, 2570.
[73] Y. Wu, F. Xie, H. Chen, X. Yang, H. Su, M. Cai, Z. Zhou, T. Noda, L. Han, *Adv. Mater.* **2017**, *29*, 1701073.
[74] D. Di Girolamo, F. Di Giacomo, F. Matteocci, A. G. Marrani, D. Dini, A. Abate, *Chem. Sci.* **2020**, *11*, 7746.
[75] S. Sajid, A. M. Elseman, H. Huang, J. Ji, S. Dou, H. Jiang, X. Liu, D. Wei, P. Cui, M. Li, *Nano Energy* **2018**, *51*, 408.
[76] W. Chen, B. Han, Q. Hu, M. Gu, Y. Zhu, W. Yang, Y. Zhou, D. Luo, F.-Z. Liu, R. Cheng, R. Zhu, S.-P. Feng, A. B. Djurišić, T. P. Russell, Z. He, *Sci. Bull.* **2021**, *66*, 991.
[77] W. Chen, L. Xu, X. Feng, J. Jie, Z. He, *Adv. Mater.* **2017**, *29*, 1603923.
[78] W. Chen, G. Zhang, L. Xu, R. Gu, Z. Xu, H. Wang, Z. He, *Mater. Today Energy* **2016**, *1–2*, 1.
[79] W. Chen, Y. Wu, J. Fan, A. B. Djurišić, F. Liu, H. W. Tam, A. Ng, C. Surya, W. K. Chan, D. Wang, Z.-B. He, *Adv. Energy Mater.* **2018**, *8*, 1703519.
[80] W. Chen, Y. Zhou, L. Wang, Y. Wu, B. Tu, B. Yu, F. Liu, H.-W. Tam, G. Wang, A. B. Djurišić, L. Huang, Z. He, *Adv. Mater.* **2018**, *30*, 1800515.
[81] W. Chen, Y. Zhou, G. Chen, Y. Wu, B. Tu, F.-Z. Liu, L. Huang, A. M. C. Ng, A. B. Djurišić, Z. He, *Adv. Energy Mater.* **2019**, *9*, 1803872.
[82] D. Tiwari, O. S. Hutter, G. Longo, *J. Phys. Energy* **2021**, *3*, 034010.
[83] X. Liu, Y. Cheng, B. Tang, Z. G. Yu, M. Li, F. Lin, S. Zhang, Y.-W. Zhang, J. Ouyang, H. Gong, *Nano Energy* **2020**, *71*, 104556.
[84] G. Tang, P. You, Q. Tai, A. Yang, J. Cao, F. Zheng, Z. Zhou, J. Zhao, P. K. L. Chan, F. Yan, *Adv. Mater.* **2019**, 1807689.
[85] X. Li, J. Yang, Q. Jiang, H. Lai, S. Li, Y. Tan, Y. Chen, S. Li, *J. Mater. Chem. A* **2019**, *7*, 7065.
[86] A. D. Taylor, Q. Sun, K. P. Goetz, Q. An, T. Schramm, Y. Hofstetter, M. Litterst, F. Paulus, Y. Vaynzof, *Nat. Commun.* **2021**, *12*, 1.
[87] X. L. Trinh, H. C. Kim, *Energy Reports* **2020**, *6*, 1297.
[88] D. Chen, S. Pang, W. Zhu, H. Zhang, L. Zhou, F. He, J. Chang, Z. Lin, H. Xi, J. Zhang, C. Zhang, Y. Hao, *J. Nanomater.* **2018**, *2018*, https://doi.org/10.1155/2018/4012850.
[89] L. Lin, C. Gu, J. Zhu, Q. Ye, E. Jiang, W. Wang, M. Liao, Z. Yang, Y. Zeng, J. Sheng, W. Guo, B. Yan, P. Gao, J. Ye, Y. Zhu, *J. Mater. Sci.* **2019**, *54*, 7789.
[90] H. B. Michaelson, *J. Appl. Phys.* **1977**, *48*, 4729.
[91] K. Domanski, J. P. Correa-Baena, N. Mine, M. K. Nazeeruddin, A. Abate, M. Saliba, W. Tress, A. Hagfeldt, M. Grätzel, *ACS Nano* **2016**, *10*, 6306.
[92] C. Besleaga, L. E. Abramiuc, V. Stancu, A. G. Tomulescu, M. Sima, L. Trinca, N. Plugaru, L. Pintilie, G. A. Nemnes, M. Iliescu, H. G. Svavarsson, A. Manolescu, I. Pintilie, *J. Phys. Chem. Lett.* **2016**, *7*, 5168.
[93] H. Li, R. Yang, C. Wang, Y. Wang, H. Chen, H. Zheng, D. Liu, T. Zhang, F. Wang, P. Gu, J. Wu, Z. D. Chen, P. Zhang, S. Li, *IEEE J. Photovoltaics* **2019**, *9*, 1081.
[94] S. Svanström, T. J. Jacobsson, G. Boschloo, E. M. J. Johansson, H. Rensmo, U. B. Cappel, *ACS Appl. Mater. Interfaces* **2020**, *12*, 7212.
[95] S. Cacovich, L. Ciná, F. Matteocci, G. Divitini, P. A. Midgley, A. Di Carlo, C. Ducati, *Nanoscale* **2017**, *9*, 4700.
[96] N. N. Shlenskaya, N. A. Belich, M. Grätzel, E. A. Goodilin, A. B. Tarasov, *J. Mater. Chem. A* **2018**, *6*, 1780.
[97] C. Wu, K. Wang, Y. Jiang, D. Yang, Y. Hou, T. Ye, C. S. Han, B. Chi, L. Zhao, S. Wang, W. Deng, S. Priya, *Adv. Funct. Mater.* **2021**, *31*, 1.
[98] G. Zhang, P. Xie, Z. Huang, Z. Yang, Z. Pan, Y. Fang, H. Rao, X. Zhong, *Adv. Funct. Mater.* **2021**, *2011187*, 1.
[99] Y. Wu, S. Wang, T. Ouyang, W. Li, M. Chen, Y. Lu, P. Qi, Y. Tang, *Nanotechnology* **2021**, *32*, https://doi.org/10.1088/1361-6528/abe891.
[100] Q. Q. Chu, Z. Sun, B. Ding, K. sik Moon, G. J. Yang, C. P. Wong, *Nano Energy* **2020**, *77*, 105110.
[101] X. Chen, Y. Xia, Q. Huang, Z. Li, A. Mei, Y. Hu, T. Wang, R. Cheacharoen, Y. Rong, H. Han, *Adv. Energy Mater.* **2021**, https://doi.org/10.1002/aenm.202100292.
[102] M. Guo, J. Liu, Y. Yuan, Z. Zhang, S. Yin, J. Leng, N. Huang, *J. Photochem. Photobiol. A Chem.* **2020**, *403*, 112843.
[103] R. Chen, Y. Feng, C. Zhang, M. Wang, L. Jing, C. Ma, J. Bian, Y. Shi, *J. Mater. Chem. C* **2020**, *8*, 9262.
[104] M. Tian, C. Y. Woo, J. W. Choi, J. Y. Seo, J. M. Kim, S. H. Kim, M. Song, H. W. Lee, *ACS Appl. Mater. Interfaces* **2020**, *12*, 54806.
[105] R. Chen, Y. Feng, L. Jing, M. Wang, H. Ma, J. Bian, Y. Shi, *J. Mater. Chem. C* **2021**, *9*, 3546.
[106] L. Lin, P. Li, Z. Kang, H. Xiong, Y. Chen, Q. Yan, L. Jiang, Y. Qiu, *Adv. Theory Simulations* **2021**, *4*, 1.
[107] S. He, L. Qiu, D. Y. Son, Z. Liu, E. J. Juarez-Perez, L. K. Ono, C. Stecker, Y. Qi, *ACS Energy Lett.* **2019**, *4*, 2032.
[108] Z. Gong, B. He, J. Zhu, X. Yao, S. Wang, H. Chen, Y. Duan, Q. Tang, *Sol. RRL* **2021**, *5*, 1.
[109] X. Zhang, J. Yang, L. Xie, X. Lu, X. Gao, J. Gao, L. Shui, S. Wu, J. M. Liu, *Dye. Pigment.* **2021**, *186*, 109024.
[110] D. Bogachuk, S. Zouhair, K. Wojciechowski, B. Yang, V. Babu, L. Wagner, B. Xu, J. Lim, S. Mastroianni, H. Pettersson, A. Hagfeldt, A. Hinsch, *Energy Environ. Sci.* **2020**, *13*, 3880.
[111] F. Yang, L. Dong, D. Jang, B. Saparov, K. C. Tam, K. Zhang, N. Li, C. J. Brabec, H.-J. Egelhaaf, *Adv. Energy Mater.* **2021**, 2101219.
[112] S. Alon, M. Sohmer, C. S. Pathak, I. Visoly-Fisher, L. Etgar, *Sol. RRL* **2021**, *5*, 2100028.
[113] H. Liu, Y. Xie, P. Wei, W. Wang, H. Chen, C. Geng, Y. Qiang, *J. Alloys Compd.* **2020**, *842*, 155851.
[114] S. Pitchaiya, N. Eswaramoorthy, M. Natarajan, A. Santhanam, V. Asokan, V. Madurai Ramakrishnan, B. Rangasamy, S. Sundaram, P. Ravirajan, D. Velauthapillai, *Sci. Rep.* **2020**, *10*, 1.

[115] S. S. Mali, H. Kim, J. V. Patil, C. K. Hong, *ACS Appl. Mater. Interfaces* **2018**, *10*, 31280.
[116] V. Babu, R. Fuentes Pineda, T. Ahmad, A. O. Alvarez, L. A. Castriotta, A. Di Carlo, F. Fabregat-Santiago, K. Wojciechowski, *ACS Appl. Energy Mater.* **2020**, *3*, 5126.
[117] Q. Luo, H. Ma, Q. Hou, Y. Li, J. Ren, X. Dai, Z. Yao, Y. Zhou, L. Xiang, H. Du, H. He, N. Wang, K. Jiang, H. Lin, H. Zhang, Z. Guo, *Adv. Funct. Mater.* **2018**, *28*, 1.
[118] H. Xie, X. Yin, Y. Guo, D. Liu, T. Liang, G. Wang, W. Que, *Nanotechnology* **2020**, *32*, https://doi.org/10.1088/1361-6528/abcf70.
[119] C. O. Teixeira, L. Andrade, A. Mendes, *J. Power Sources* **2020**, *479*, 1.
[120] P. Panneerselvam, S. Angaiah, *New J. Chem.* **2021**, *45*, 423.
[121] J. Li, J. Duan, J. Du, X. Yang, Y. Wang, P. Yang, Y. Duan, Q. Tang, *ACS Appl. Mater. Interfaces* **2020**, *12*, 47408.
[122] B. Wang, N. Li, L. Yang, C. Dall'agnese, A. K. Jena, S. I. Sasaki, T. Miyasaka, H. Tamiaki, X. F. Wang, *J. Am. Chem. Soc.* **2021**, *143*, 2207.
[123] D. Song, L. Y. Hsu, C.-M. Tseng, E. W.-G. Diau, *Mater. Adv.* **2021**, *2*, 754.
[124] M. Ahmadi, Y.-C. Hsiao, T. Wu, Q. Liu, W. Qin, B. Hu, *Adv. Energy Mater.* **2017**, *7*, 1601575.
[125] S. A. Ok, B. Jo, S. Somasundaram, H. J. Woo, D. W. Lee, Z. Li, B.-G. Kim, J. H. Kim, Y. J. Song, T. K. Ahn, S. Park, H. J. Park, *Nat. Commun.* **2018**, *9*, 4537.
[126] B. Jo, H. Park, E. Kamaraj, S. Lee, B. Jung, S. Somasundaram, G. G. Jeon, K.-T. Lee, N. Kim, J. H. Kim, B.-G. Kim, T. K. Ahn, S. Park, H. J. Park, *Adv. Funct. Mater.* **2021**, *31*, 2007180.
[127] J. Park, S. E. Yoon, J. Lee, D. R. Whang, S. Y. Lee, S. J. Shin, J. M. Han, H. Seo, H. J. Park, J. H. Kim, B.-G. Kim, *Adv. Funct. Mater.* **2020**, *30*, 2001560.
[128] X. Lin, D. Cui, X. Luo, C. Zhang, Q. Han, Y. Wang, L. Han, *Energy Environ. Sci.* **2020**, *13*, 3823.
[129] W. Chen, K. Li, Y. Wang, X. Feng, Z. Liao, Q. Su, X. Lin, Z. He, *J. Phys. Chem. Lett.* **2017**, *8*, 591.
[130] Q. Hu, W. Chen, W. Yang, Y. Li, Y. Zhou, B. W. Larson, J. C. Johnson, Y.-H. Lu, W. Zhong, J. Xu, L. Klivansky, C. Wang, M. Salmeron, A. B. Djurišić, F. Liu, Z. He, R. Zhu, T. P. Russell, *Joule* **2020**, *4*, 1575.
[131] C.-C. Chang, J.-H. Tao, C.-E. Tsai, Y.-J. Cheng, C.-S. Hsu, *ACS Appl. Mater. Interfaces* **2018**, *10*, 21466.
[132] M.-H. Tremblay, K. Schutt, Y. Zhang, J. Lim, Y.-H. Lin, J. H. Warby, S. Barlow, H. J. Snaith, S. R. Marder, *Sustain. Energy Fuels* **2020**, *4*, 190.
[133] D. Vaitukaitytė, A. Al-Ashouri, M. Daškevičienė, E. Kamarauskas, J. Nekrasovas, V. Jankauskas, A. Magomedov, S. Albrecht, V. Getautis, *Sol. RRL* **2021**, *5*, 2000597.
[134] L. Wang, F. Zhang, T. Liu, W. Zhang, Y. Li, B. Cai, L. He, Y. Guo, X. Yang, B. Xu, J. M. Gardner, L. Kloo, L. Sun, *J. Energy Chem.* **2021**, *55*, 211.
[135] J. Wu, M. Hu, L. zhang, G. Song, Y. Li, W. Tan, Y. Tian, B. Xu, *Chem. Eng. J.* **2021**, *422*, 130124.
[136] J.-Y. Shao, B. Yu, Y.-D. Wang, Z.-R. Lan, D. Li, Q. Meng, Y.-W. Zhong, *ACS Appl. Energy Mater.* **2020**, *3*, 5058.
[137] K. Rakstys, M. Stephen, J. Saghaei, H. Jin, M. Gao, G. Zhang, K. Hutchinson, A. Chesman, P. L. Burn, I. Gentle, P. E. Shaw, *ACS Appl. Energy Mater.* **2020**, *3*, 889.
[138] H. Kwon, J. W. Lim, J. Han, L. N. Quan, D. Kim, E.-S. Shin, E. Kim, D.-W. Kim, Y.-Y. Noh, I. Chung, D. H. Kim, *Nanoscale* **2019**, *11*, 19586.
[139] H. Zhu, Y. Ren, L. Pan, O. Ouellette, F. T. Eickemeyer, Y. Wu, X. Li, S. Wang, H. Liu, X. Dong, S. M. Zakeeruddin, Y. Liu, A. Hagfeldt, M. Grätzel, *J. Am. Chem. Soc.* **2021**, *143*, 3231.
[140] J. Luo, J. Xia, H. Yang, H. A. Malik, F. Han, H. Shu, X. Yao, Z. Wan, C. Jia, *Nano Energy* **2020**, *70*, 104509.
[141] Z. Li, B. H. Jo, S. J. Hwang, T. H. Kim, S. Somasundaram, E. Kamaraj, J. Bang, T. K. Ahn, S. Park, H. J. Park, *Adv. Sci.* **2019**, *6*, 1802163.
[142] B. Wang, F. Wu, S. Bi, J. Zhou, J. Wang, X. Leng, D. Zhang, R. Meng, B. Xue, C. Zong, L. Zhu, Y. Zhang, H. Zhou, *J. Mater. Chem. A* **2019**, *7*, 23895.
[143] E. H. Jung, N. J. Jeon, E. Y. Park, C. S. Moon, T. J. Shin, T.-Y. Yang, J. H. Noh, J. Seo, *Nature* **2019**, *567*, 511.
[144] F. Di Giacomo, S. Razza, F. Matteocci, A. D'Epifanio, S. Licoccia, T. M. Brown, A. Di Carlo, *J. Power Sources* **2014**, *251*, 152.
[145] N. Yaghoobi Nia, M. Bonomo, M. Zendehdel, E. Lamanna, M. M. H. Desoky, B. Paci, F. Zurlo, A. Generosi, C. Barolo, G. Viscardi, P. Quagliotto, A. Di Carlo, *ACS Sustain. Chem. Eng.* **2021**, *9*, 5061.
[146] N. Y. Nia, F. Matteocci, L. Cina, A. Di Carlo, *ChemSusChem* **2017**, *10*, 3854.
[147] M. Kim, S. G. Motti, R. Sorrentino, A. Petrozza, *Energy Environ. Sci.* **2018**, *11*, 2609.
[148] B. Chaudhary, A. Kulkarni, A. K. Jena, M. Ikegami, Y. Udagawa, H. Kunugita, K. Ema, T. Miyasaka, *ChemSusChem* **2017**, *10*, 2473.
[149] P. J. S. Rana, R. K. Gunasekaran, S. H. Park, V. Tamilavan, S. Karuppanan, H.-J. Kim, K. Prabakar, *J. Phys. Chem. C* **2019**, *123*, 8560.
[150] P. Topolovsek, F. Lamberti, T. Gatti, A. Cito, J. M. Ball, E. Menna, C. Gadermaier, A. Petrozza, *J. Mater. Chem. A* **2017**, *5*, 11882.
[151] A. Magomedov, A. Al-Ashouri, E. Kasparavičius, S. Strazdaite, G. Niaura, M. Jošt, T. Malinauskas, S. Albrecht, V. Getautis, *Adv. Energy Mater.* **2018**, *8*, 1801892.
[152] E. Aktas, N. Phung, H. Köbler, D. A. González, M. Méndez, I. Kafedjiska, S.-H. Turren-Cruz, R. Wenisch, I. Lauermann, A. Abate, E. Palomares, *Energy Environ. Sci.* **2021**, *14*, 3976.
[153] E. Li, C. Liu, H. Lin, X. Xu, S. Liu, S. Zhang, M. Yu, X.-M. Cao, Y. Wu, W.-H. Zhu, *Adv. Funct. Mater.* **2021**, 2103847.
[154] A. Al-Ashouri, A. Magomedov, M. Roß, M. Jošt, M. Talaikis, G. Chistiakova, T. Bertram, J. A. Márquez, E. Köhnen, E. Kasparavičius, S. Levcenco, L. Gil-Escrig, C. J. Hages, R. Schlatmann, B. Rech, T. Malinauskas, T. Unold, C. A. Kaufmann, L. Korte, G. Niaura, V. Getautis, S. Albrecht, *Energy Environ. Sci.* **2019**, *12*, 3356.
[155] A. Al-Ashouri, E. Köhnen, B. Li, A. Magomedov, H. Hempel, P. Caprioglio, J. A. Márquez, A. B. Morales Vilches, E. Kasparavicius, J. A. Smith, N. Phung, D. Menzel, M. Grischek, L. Kegelmann, D. Skroblin, C. Gollwitzer, T. Malinauskas, M. Jošt, G. Matič, B. Rech, R. Schlatmann, M. Topič, L. Korte, A. Abate, B. Stannowski, D. Neher, M. Stolterfoht, T. Unold, V. Getautis, S. Albrecht, *Science (80-.).* **2020**, *370*, 1300 LP.
[156] M. Kim, A. Alfano, G. Perotto, M. Serri, N. Dengo, A. Mezzetti, S. Gross, M. Prato, M. Salerno, A. Rizzo, R. Sorrentino, E. Cescon, G. Meneghesso, F. Di Fonzo, A. Petrozza, T. Gatti, F. Lamberti, *Commun. Mater.* **2021**, *2*, 6.
[157] M. De Bastiani, A. J. Mirabelli, Y. Hou, F. Gota, E. Aydin, T. G. Allen, J. Troughton, A. S. Subbiah, F. H. Isikgor, J. Liu, L. Xu, B. Chen, E. Van Kerschaver, D. Baran, B. Fraboni, M. F. Salvador, U. W. Paetzold, E. H. Sargent, S. De Wolf, *Nat. Energy* **2021**, *6*, 167.
[158] S. Sansoni, M. De Bastiani, E. Aydin, E. Ugur, F. H. Isikgor, A. Al-Zahrani, F. Lamberti, F. Laquai, M. Meneghetti, S. De Wolf, *Adv. Mater. Technol.* **2020**, *5*, https://doi.org/10.1002/admt.201901009.
[159] K. K. Wang, Z. Z. Wu, C. J. Peng, K. P. Wang, B. Cheng, C. L. Song, G. R. Han, Y. Liu, *Sol. Energy Mater. Sol. Cells* **2015**, *143*, 198.

Francesco Lamberti obtained his Ph.D. in material sciences and engineering from the University of Padova in 2011. After studying electrochemical biosensors on optically transparent electrodes, he moved to the Italian Institute of Technology (IIT) in Milano, working in the group of Dr. Annamaria Petrozza on the development of perovskite solar cells. Currently, he holds a research position at the University of Padova focusing on thin-film processing for emerging photovoltaics exploiting ultrasonic spraying system.

Zhu-Bing He obtained his Ph.D. in physics and materials science from City University of Hong Kong in 2009. He joined as an associate professor in the Department of Materials Science and Engineering of Southern University of Science and Technology in 2012, after working as a research scientist to develop HIT photovoltaics in industry. Currently, he focuses on interface science and engineering in solar conversion topics, especially high-efficient hybrid and heterojunction solar cells, spectrum splitting and accumulation of solar photons via nanophotonics, and heat transfer in fluid and phase-change materials.

Teresa Gatti holds a master's degree in chemistry from the University of Bologna, Italy (2008) and a Ph.D. in materials engineering from Politecnico di Milano, Italy (2014). After postdoctoral activities at the Department of Chemical Sciences of the University of Padova (Italy), since 2019, she has been a group leader at the Center for Materials Research of the Justus Liebig University Giessen (Germany). Her research interests cover the production, processing, and application in optoelectronic devices of different emerging semiconducting materials, with special attention to species based on noncritical elements and featuring low-environmental impact.